

UNCLASSIFIED

AD NUMBER
ADB047311
NEW LIMITATION CHANGE
TO Approved for public release, distribution unlimited
FROM Distribution authorized to U.S. Gov't. agencies only; Test and Evaluation; Jun 1979. Other requests shall be referred to the Air Force Materials Laboratory, Nonmetallic Materials Division, Attn: MBC, Wright-Patterson AFB, OH 45433.
AUTHORITY
AFWAL ltr, 31 May 1985

THIS PAGE IS UNCLASSIFIED

OFFICIAL FILE COPY

AFML-TR-78-164

Part II

ADB047311

**PHYSICAL CHEMICAL PROPERTIES OF COMPLEX
AROMATIC-HETEROCYCLIC POLYMERS**

*G. C. BERRY
E. F. CASASSA
P. METZGER
S. VENKATRAMEN*

*CARNEGIE-MELLON UNIVERSITY
4400 FIFTH AVENUE
PITTSBURGH, PENNSYLVANIA 15213*

JANUARY 1980

TECHNICAL REPORT AFML-TR-78-164 Part II
Final Report for period June 1977 — June 1979

Distribution limited to U.S. Government agencies only; Test and Evaluation June 1979.
Other requests for this document must be referred to the Air Force Materials Laboratory,
Nonmetallic Materials Division, AFML/MBC, Wright-Patterson Air Force Base, Ohio 45433.

AIR FORCE MATERIALS LABORATORY
AIR FORCE WRIGHT AERONAUTICAL LABORATORIES
AIR FORCE SYSTEMS COMMAND
WRIGHT-PATTERSON AIR FORCE BASE, OHIO 45433

20040226256

BEST AVAILABLE COPY

NOTICE

When Government drawings, specifications, or other data are used for any purpose other than in connection with a definitely related Government procurement operation, the United States Government thereby incurs no responsibility nor any obligation whatsoever; and the fact that the government may have formulated, furnished, or in any way supplied the said drawings, specifications, or other data, is not to be regarded by implication or otherwise as in any manner licensing the holder or any other person or corporation, or conveying any rights or permission to manufacture, use, or sell any patented invention that may in any way be related thereto.

This technical report has been reviewed and is approved for publication.

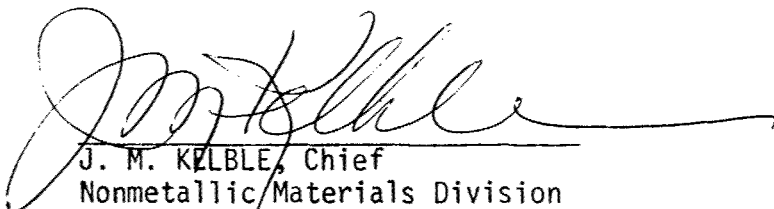


Project Monitor

FOR THE COMMANDER



T. J. REINHART, JR., Chief
Composites, Adhesives & Fibrous
Materials Branch
Nonmetallic Materials Division



J. M. KELBLE, Chief
Nonmetallic Materials Division

Copies of this report should not be returned unless return is required by security considerations, contractual obligations, or notice on a specific document.

UNCLASSIFIED

SECURITY CLASSIFICATION OF THIS PAGE (When Data Entered)

REPORT DOCUMENTATION PAGE		READ INSTRUCTIONS BEFORE COMPLETING FORM
1. REPORT NUMBER AFML-TR-78-164, PT II	2. GOVT ACCESSION NO.	3. RECIPIENT'S CATALOG NUMBER
4. TITLE (and Subtitle) "Physical Chemical Properties of Complex Aromatic-Heterocyclic Polymers"		5. TYPE OF REPORT & PERIOD COVERED Final Report June 1977/June 1979
		6. PERFORMING ORG. REPORT NUMBER
7. AUTHOR(s) G. C. Berry, Principal Investigator E. F. Casassa P. Metzger and S. Venkatramen		8. CONTRACT OR GRANT NUMBER(s) F33615-77-C-5165
9. PERFORMING ORGANIZATION NAME AND ADDRESS Carnegie-Mellon University 4400 Fifth Avenue Pittsburgh, PA 15213		10. PROGRAM ELEMENT, PROJECT, TASK AREA & WORK UNIT NUMBERS 24190403
11. CONTROLLING OFFICE NAME AND ADDRESS Air Force Materials Laboratory (AFML/MBC) Air Force Wright Aeronautical Laboratories Wright-Patterson AFB, Ohio 45433		12. REPORT DATE November 1979
		13. NUMBER OF PAGES 95
14. MONITORING AGENCY NAME & ADDRESS (if different from Controlling Office)		15. SECURITY CLASS. (of this report) UNCLASSIFIED
		15a. DECLASSIFICATION/DOWNGRADING SCHEDULE
16. DISTRIBUTION STATEMENT (of this Report) Disribution limited to U.S. Governement agencies only; test and evaluation, June 1979. Other requests for this document must be referred to the Air Force Materials Laboratory, Nonmetallic Materials Division, Composites, Adhesives and Fibrous Materials Branch, AFML/MBC, Wright-Patterson Air Force Base, Ohio 45433.		
17. DISTRIBUTION STATEMENT (of the abstract entered in Block 20, if different from Report)		
18. SUPPLEMENTARY NOTES		
19. KEY WORDS (Continue on reverse side if necessary and identify by block number) PHYSICAL CHEMICAL PROPERTIES AROMATIC HETEROCYCLIC POLYMERS		
20. ABSTRACT (Continue on reverse side if necessary and identify by block number) Physical chemical methods have been used to characterize poly(1-4, phenylene bisoxazole), PBO, and poly(1-4, phenylene bithiazole), PBT, by studies on dilute solutions. Experimental methods include absolute intensity and intensity fluctuation light scattering, viscometry, and absorption and fluorescence spectroscopy. Both PBO and PBT are soluble only in strong, protic acids, in which the solvated chains are strongly protonated. Consequently, the measured properties depend markedly on the ionic strength of the solvent. The		

DD FORM 1 JAN 73 1473

EDITION OF 1 NOV 65 IS OBSOLETE

UNCLASSIFIED

SECURITY CLASSIFICATION OF THIS PAGE (When Data Entered)

UNCLASSIFIED

SECURITY CLASSIFICATION OF THIS PAGE(When Data Entered)

data show that PBO and PBT are rodlike chains, but the analysis is complicated by the tendency of both to undergo interchain association. The latter effect is more pronounced with PBO than with PBT. The association is not an equilibrium process. It is necessary to combine the results of several kinds of experiments to assess the effects of the metastable association, and to elucidate the molecular structure.

UNCLASSIFIED

SECURITY CLASSIFICATION OF THIS PAGE(When Data Entered)

FOREWORD

This report was prepared at Mellon Institute, Carnegie-Mellon University, 4400 Fifth Avenue, Pittsburgh, Pennsylvania 15213, under AFML Contract No. F33615-77-C-5165. It was administered under the direction of the Air Force Materials Laboratory, Dr. T. E. Helminiak.

The report covers work conducted from 30 June 1977 to 30 June 1979. It was submitted in November, 1979. Authors are G. C. Berry, Principal Investigator, E. F. Casassa, P. Metzger, and S. Venkatramen from CMU.

TABLE OF CONTENTS

1. INTRODUCTION	1
2. PHYSICAL CHEMICAL CHARACTERIZATION METHODS	3
3. EXPERIMENTAL	15
1. Absolute Intensity Light Scattering	15
2. Intensity Fluctuation Light Scattering	17
3. Fluorescence Measurements	22
4. Intrinsic Viscosity	26
5. Exclusion Chromatography	26
4. RESULTS AND DISCUSSION	28
1. The Effects of Ionic Strength	28
2. Exclusion Chromatography	35
3. Fluorescence and Absorption	38
4. Effects of Centrifugation	54
5. Estimates of the Rod Length	59
6. Phase Equilibria in Moderately Concentrated Solutions	62
5. CONCLUSIONS AND SUMMARY	69
REFERENCES	71
APPENDIX	72

LIST OF TABLES

Table		Page
1	Exclusion chromatography data obtained on several PBO polymers original and after precipitation from methane sulfonic acid solution.	40
2	Extinction coefficient $\mu_{632.8}$; and K^0 from intercepts of Figures 15 and 16.	52
3	Summary of average length of PBO and PBT polymers.	60
4	Temperature and concentration ranges for biphasic solution in PBO and PBT polymers.	67

LIST OF ILLUSTRATIONS

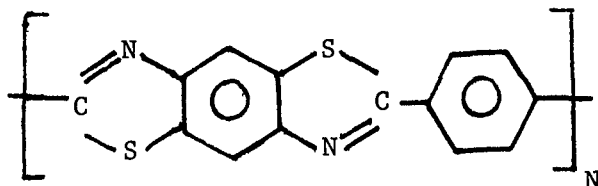
Figure		Page
1	Schematic diagram of IFLS instrument.	18
2	The log of the correlation function and coherence factor f (γ in text) for various combinations of lens, pinhole and number of averages for polystyrene in decalin.	21
3	Sample cell used for IFLS measurement allowing adjustment of vertical position.	23
4	The slope of the log of the correlation function $c(t)$ versus $\sin^2\theta/2$ for a narrow distribution polystyrene sample in methyl ethyl ketone. Open circles--without added dye, half-filled circles--with added crystal violet dye.	24
5	Light scattering data on PBT-20 in methane sulfonic acid (filled symbols) and chlorosulfonic acid (unfilled symbols).	29
6	η_{sp}/c versus concentration for four PBO polymers in methane sulfonic acid (filled symbols) and chlorosulfonic acid (unfilled symbols).	31
7	$D_{M\eta}$ for CMU PBO 160/8 in methane sulfonic acid (unfilled symbols), chlorosulfonic acid (filled symbols) and chlorosulfonic acid with added lithium chlorosulfonate (half-filled symbols).	34
8	Exclusion chromatography obtained on several PBO polymers in MSA. Left to right: CMU 160/8, Celanese 9A, AFML 2, AFML 5, Celanese 3, and AFML 6.	36
9	Exclusion chromatography obtained for SRI PBI 20. Absorption of the eluent at 440 nm versus elution volume V_e and $\log M$.	37
10	Absorption spectra of AFML PBO-5 (solid line) and CMU PBO 160/8 (dashed line) showing differences at long wavelengths.	39
11	Absorption spectra of several PBO polymers in the long wavelength region.	42
12	Absorption spectra at long wavelength for a series of aliquots removed from a polymerization in PPA at 160°C.	43
13	Fluorescence emission spectra obtained for CMU PBO 160/4 in methane sulfonic acid with excitation at the wavelengths indicated.	45

List of Illustrations (continued)

Figure		Page
14	$\ln(R_p^F/c)$ versus concentration in methane sulfonic acid (see Eqn. 36 in text) for two early aliquots removed from a polymerization in PPA at 160°C. Excitation at 514.5 nm, emission at 686 nm.	46
15	$\ln(R_p^F/c)$ versus concentration for several PBO polymers in chlorosulfonic acid. Excitation at 632.8 nm. Circles with pips clockwise from top: AFML PBO 30, AFML PBO 9, AFML PBO 2, and AFML PBO 6. Triangles: CMU PBO 160/8; squares: Celanese PBO 3 and diamonds: Celanese PBO 9A.	48
16	$\ln(R_p^F/c)$ versus concentration for several PBO polymers in methane sulfonic acid. Excitation at 632.8 nm. Circles with pips clockwise from left: AFML PBO 6, AFML PBO 5 and AFML PBO 9. Triangles: CMU PBO 160/8.	49
17	$\ln(R_p^F/c)$ versus concentration for two PBT polymers. Excitation at 632.8 nm. Triangles: SRI PBT 20; pips left: chlorosulfonic acid, pips right, methane sulfonic acid. Circles: SRI PBT 23; pips down: chlorosulfonic acid; pips right: methane sulfonic acid.	50
18	Reciprocal total scattering (U_V) and depolarized scattering (H_V) from vertically polarized incident beam for CMU PBO 160/8 in methane sulfonic acid.* Circles: uncentrifuged triangles: after centrifugation 16 hours at 5,000 G. $c = 0.045$ g/dl	55
19	Reciprocal scattering for CMU PBO 160/8 in chlorosulfonic acid. Symbols the same as in Fig. 18.	56
20	D_{Mn} for CMU PBO 160/8 in methane sulfonic acid after centrifugation. Pips up: upper portion of cell; pips down: lower portion of cell.	58
21	Cell for observation of phase changes.	64
22	Temperature and concentration limits of the biphasic region for PBT solutions.	66

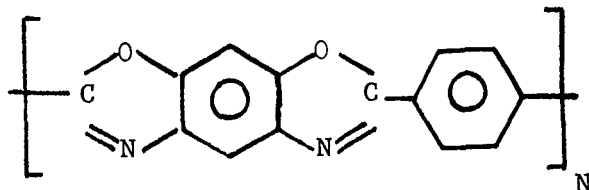
1. INTRODUCTION

The following is a report of work completed under AFML contract No. F33615-77-C-5165 for the period ending 30 June 1979. The study involves the physical chemical properties of the poly(1,4 phenylene benzbisthiazole)



PBT

and the poly (1,4 phenylene benzbisoxazole)



PBO

This report will include polymer characterization by means of absolute intensity light scattering (AALS), intensity fluctuation light scattering (IFLS), electronic absorption and fluorescence spectroscopy, viscometry, and exclusion (or gel permeation) chromatography (GPC), and studies of the phase equilibria of moderately concentrated solutions.

Both PBO and PBT have a rodlike chain conformation, exhibit

limited solubility, and will form nematic liquid crystalline solutions under appropriate conditions. Information on molecular conformation, chain dimensions, interchain interaction and interchain association is important to the understanding of the behavior of PBO and PBT, and will be elucidated by the characterization studies with dilute solutions. The studies of phase equilibria will provide information on the order-disorder transition for comparison with theoretical predictions.

In the following section, a number of equations used in the analysis of physical chemical data on dilute solutions are gathered together for easy reference, and to permit an overall perspective of the nature of the study.

2. PHYSICAL CHEMICAL CHARACTERIZATION METHODS

Physical chemical characterization of PBO and PBT by studies of dilute solutions will involve the following experimental parameters:

M	the molecular weight
R_G	the root of the mean square radius of gyration
A_2	the second virial coefficient
δ	the molecular optical anisotropy
Ξ^0	the translational friction coefficient (at infinite dilution, denoted by superscript 0)
R_H	a hydrodynamic radius, defined as $\Xi^0/6\pi\eta_s$, with η_s the solvent viscosity
D_R^0	the rotatory diffusion constant (at infinite dilution)
$[\eta]$	the intrinsic viscosity defined as $\lim_{c \rightarrow 0} (\eta - \eta_s)/\eta_s c$, with η the viscosity for concentration c
μ_λ	the extinction coefficient for absorption at wavelength λ
K_λ^0	the quantum yield for fluorescence with wavelength λ
K_λ^Q	the Perrin self-extinction for fluorescence with wavelength λ
r	the fluorescence emission anisotropy

In the analysis of experimental data, it will be convenient to refer to the predictions of the wormlike chain model, which involves, in addition to the above, the characterization parameters:

- ρ the persistence length
 L the chain contour length, equal to M/M_L with M_L the mass per unit length
 δ_0 the intrinsic optical anisotropy of the (presumed) cylindrical scattering elements
 d_H the hydrodynamic diameter of a chain element
 d_T the thermodynamic diameter of a chain element

In our discussion M_L will be calculated as m_0/ℓ , with m_0 the mass of a repeat unit with length ℓ . For example, values of $m_0 = 234$, $\ell = 12.8$ A and $M_L = 18.3$ A⁻¹ for PBO and $m_0 = 266$, $\ell = 12.1$ and $M_L = 22.0$ A⁻¹ for PBT will be used. For the wormlike chain model, which reduces to the rodlike model for small L/ρ ,¹⁻⁶

$$R_G^2 = \frac{L^2}{12} W(L/\rho) \quad (1a)$$

$$W(Z) = (4/Z) \{1 - 3Z^{-1} + 6Z^{-2} - 6Z^{-3} [1 - \exp(-Z)]\} \quad (1b)$$

$$\delta^2 = \delta_0^2 Y(L/\rho) \quad (2a)$$

$$Y(Z) = (2/3Z) \{1 - (3Z)^{-1} [1 - \exp(-3Z)]\} \quad (2b)$$

$$A_2 = A_2^0 [1 + b_1(L/\rho)\zeta + \dots] \quad (3a)$$

$$MA_2^0 = \frac{\pi}{4} N_A d_T L^{-1} \quad (3b)$$

$$\zeta = M_A^2 \lambda / 4\pi^{3/2} N_A R_G^3 \quad (3c)$$

$$R_H = \bar{M}^0 / 6\pi \eta_s = \frac{L}{2} H^{-1}(L/\rho, L/d_H) \quad (4a)$$

$$\lim_{L/\rho \rightarrow 0} H(L/\rho, L/d_H) = H(L/d_H) \quad (4b)$$

$$H(X) = \ln X + 0.3863 + 0.04167 \frac{12 + \ln X}{X} - 0.0625X^{-2} + \dots \quad (4c)$$

$$M[\eta] = \pi N_A R_G^2 R_H \frac{H(L/\rho, L/d_H)}{F(L/d_H)} \quad (5a)$$

$$\lim_{d/\rho < 0.1} F(X) = \ln X + 2 \ln 2 - 7/3 \quad (5b)$$

$$H(X)/F(X) \simeq 1.34 \quad (5c)$$

The first four parameters are, of course, derived from AILS experiments, whereas R_H is derived from IFLS data. Thus, with R_{Vv} and R_{Hv} the vertical and horizontal components, respectively, of the Rayleigh ratio with vertically incident light for AILS;⁷

$$[R_{Vv}(u)/KM\epsilon]^0 = (1 + \frac{4}{5} \delta^2) - \frac{1}{3} [1 - \frac{4}{5} f_1 \delta + \frac{4}{7} f_2^2 \delta^2] u + \dots (6)$$

$$[R_{Hv}(u)/KMc]^0 = \frac{3}{5} \delta^2 - \frac{9}{35} f_3^2 \delta^2 u + \dots \quad (7)$$

where $u = R_G^2 h^2$ with $h = (4\pi n/\lambda) \sin(\theta/2)$, and the superscript 0 denotes the limit of infinite dilution, and

$$R_{Vv}(0)/KMc = (1 + \frac{4}{5} \delta^2) - 2A_2 Mc + o(c^2) \quad (8)$$

$$R_{Hv}(0)/KMc = \frac{3}{5} \delta^2 + o(c^2) \quad (9)$$

The parameters f_1 , f_2 , and f_3 , which depend on L/ρ , may all be set equal to the limiting value unity for small L/ρ for our purposes.⁸

The translational diffusion coefficient is derived from IFLS measurements of the intensity correlation function $g_2(h,t)$:

$$\frac{\langle n_o n_t \rangle - \langle n \rangle^2}{\langle n \rangle^2} = g_2(h,t) \quad (10)$$

where $\langle n \rangle$ is the average photon count rate, and $\langle n_o n_t \rangle$ is the average product of photon count rates measured time t apart. For the systems studied here, we will apply the relation⁹

$$g_2(h,t) = 1 + \gamma g_1^2(h,t) \quad (11a)$$

$$g_1(h,t) = \exp(-t/2\tau_h) \quad (11b)$$

where γ is a coherence factor (see the next section), and the time constant τ_h is given by¹⁰

$$\tau_h^{-1} = 2D_M h^2 \quad (12)$$

with

$$D_M = \Xi^{-1} \frac{\partial \pi}{\partial v} \frac{1 - v_2 c}{1 - K_H v_2 c} \quad (13)$$

where

$$\Xi = \Xi^0 (1 + f(M, A_2) c + \dots) \quad (14)$$

the osmotic pressure π given by

$$\pi = kT v [1 + A_2 M c + \dots] \quad (15)$$

in terms of the number density $v = cN_A/M$ of the solute, K_H is a hydrodynamic factor and v_2 is the solute specific volume. Consequently, for small c ,

$$\lim_{c \rightarrow 0} D_M = kT/\Xi^0 \quad (16)$$

If the samples exhibit molecular weight dispersity, as is the case with the PBO and PBT polymers studied here, then the light scattering averages M^{LS} , $\langle s^2 \rangle^{LS}$, A_2^{LS} and $\Xi^{0,LS}$ are derived from

AILS and IFLS experiments. These can be related to M , R_G , etc., but for our purposes it is convenient to consider the average quantities calculated with Eqns. 1-4 for the limiting case with very small L/ρ , as this is the limit of interest with PBO and PBT. In this limit, it is convenient to define average rod lengths L_{AVG} corresponding to each of the experimental parameters:

$$L_w \equiv M^{LS}/M_L = M_w/M_L \quad (17)$$

$$L_G \equiv [12 \langle s^2 \rangle^{LS}]^{1/2} = [L_z L_{z+1}]^{1/2} \quad (18)$$

$$L_{\Xi} \equiv \left(\frac{\Xi^{0,LS} H(L/d_H)}{3\pi\eta_s L^{0.2}} \right)^{1/0.8} = \left(\frac{\Xi^{0,LS} \times 1.887}{3\pi\eta_s d^{0.2}} \right)^{1/0.8} \quad (19)$$

In the relation for L_{Ξ} , the functions $H(L, d_H)$ and $F(L/d_H)$ can be approximated by the relations

$$H(L/d_H) \approx 1.887 (L/d_H)^{0.2} \quad (20a)$$

$$F(L/d_H) \approx 1.405 (L/d_H)^{0.2} \quad (20b)$$

which provides satisfactory fit for L/d_H in the range 30 to 3000.

Use of Eqns. 19-20 requires an estimate for d_H , but since d_H enters as $d_H^{0.2}$, the estimate need not be accurate.

Similarly, an average length can be defined in terms of

$[\eta]$:

$$L_{\eta} \equiv \left(\frac{2400 F M_L [\eta]}{\pi N_A L^{0.2}} \right)^{\frac{1}{1.8}} = \left(\frac{2400 \times 1.405 M_L [\eta]}{\pi N_A d_H^{0.2}} \right)^{\frac{1}{1.8}} \quad (21a)$$

$$L_{\eta} = L_w \left(\frac{M_z}{M_w} \right)^{4/9} \quad (21b)$$

with $[\eta]$ in dl/g, where Eqn. (20b) has been used for $F(L/d_H)$ over the range of L/d_H of interest here. As with Eqns. 19-20, it is necessary to have an estimate for $d_H^{0.2}$ to compute L_{η} . An average free of this requirement is given by

$$L_{\eta, H} \equiv \left(\frac{7200 \eta_s M_L [\eta]}{H F^{-1} N_A H^{0, LS}} \right) = L_w \left(\frac{M_z}{M_w} \right)^{0.8} \quad (22)$$

Fluorescence measurements of interest include the emission anisotropy r , the lifetime τ_E of the excited state, and the absolute fluorescent intensity R^F , expressed as a Rayleigh ratio. The emission anisotropy r , given in terms of the fluorescence components R_{Vv}^F and R_{Hv}^F :

$$r = \frac{R_{Vv}^F - R_{Hv}^F}{R_{Vv}^F + 2R_{Hv}^F} \quad (23)$$

is related to the rotatory diffusion coefficient D_R for rigid particles: ¹¹

$$r = r_0 [1 + 6 D_R \tau_E]^{-1} \quad (24)$$

Here the intrinsic emission anisotropy r_0 is related to the angle β between the emission and absorbance transition vectors:

$$r_0 = \frac{1}{5} (3 \cos^2 \beta - 1) \quad (25)$$

so that r_0 is $2/5$ if β is zero.

For polydispersed systems, an average value r^F is obtained. If β and τ_E are identical for all species, and $6D_R\tau_E$ is not too large, then,

$$r^F \simeq r_0 [1 + 6D_R^F \tau_E]^{-1} \quad (26)$$

where D_R^F is the appropriately averaged value of D_R for a system with molecular weight heterogeneity (see below). For rodlike chains,¹²

$$D_R = \frac{6}{4500} \frac{RT}{\eta_s M [\eta]} \quad (27)$$

(with $[\eta]$) in dl/g, so that

$$D_R^F = \frac{6}{4500} \frac{RT}{\eta_s M_R [\eta]} \quad (28)$$

with

$$M_R^{-1} = \frac{M_n M_w M_z}{M_n M_w M_z} \int_0^{\infty} M^{-4} f(M) dM \quad (29)$$

illustrating the substantial contribution to D_R^F of short chain length

components of the distribution.

Although absorption effects are not important in measurements of r , they must be considered in studies of the quantum yield K^0 (at infinite dilution) which is related to R^F/c . (In the following R^F refers to the experimental quantity $R_{Vv}^F + R_{Hv}^F$). Two experimental arrangements are of interest:

- 1) R_p^F , the fluorescence at right angle to the incident beam, and
- 2) R_B^F , the fluorescence reflected back along the incident beam.

For the former, R^F/c is given by

$$(R_p^F/c) = \mu_\lambda K^0 \exp[-(\mu_\lambda \ell + \mu_{\lambda'} \ell' + K_q)c] \frac{\sinh(\mu_\lambda \Delta \ell / 2)}{\mu_\lambda \Delta \ell / 2} \quad (30a)$$

where λ and λ' are the wavelengths for the incident and fluorescent radiation with pathlengths ℓ and ℓ' in the sample, respectively, $\Delta \ell$ is the width of the illuminated volume viewed by the detector, and K_q is the Perrin quenching coefficient. Since $\Delta \ell$ can be made small experimentally, conditions are used such that $(\sinh x)/x$ is essentially unity (e.g., $\Delta \ell < \mu_\lambda^{-1}$), so that Eqn.(30a) becomes

$$(R_p^F/c) \simeq \mu_\lambda K^0 \exp[-(\mu_\lambda \ell + \mu_{\lambda'} \ell' + K_q)c] \quad (30b)$$

With the reflected optics,

$$\left(\frac{R_B^F}{c}\right) = \frac{\mu_\lambda K^0}{\mu_\lambda + \mu_\lambda'} \exp(-K_q c) \{1 - \exp[-(\mu_\lambda + \mu_\lambda')L]\} \quad (31a)$$

where L is the depth of the illuminated slab of solution. For large enough L (e.g., $(\mu_\lambda + \mu_\lambda')cL > 5$) Eqn. (31a) becomes

$$\frac{R_B^F}{c} \simeq \frac{\mu_\lambda K^0}{\mu_\lambda + \mu_\lambda'} \exp(-K_q c) \quad (31b)$$

so that R_B^F/c provides a measure of K_0 nearly independent of the concentration c if $K_q c$ is very small.

Relatively little information is available on K_q for polymeric solutes. According to the analysis of Perrin,¹³ K_q represents a volume within which intermolecular interactions can affect the electronic state responsible for fluorescence. Thus, K_q may provide information on intermolecular association. In part, this study is motivated by observations that R_p^F/c appears to be variable with PBO polymers at dilutions normally used for light scattering and viscosity measurements.

Exclusion chromatography provides data on the eluent concentration c as a function of the elution volume V_e . The so-called universal calibration of V_e with $M[\eta]^{14}$ that appears to be valid with flexible chain polymers provides a means of transforming V_e to M , and hence permits the estimate of M_n , M_w , M , etc, from the observed data on c and V_e . Theoretical calculations suggest that V_e might more fundamentally be a function of R_M , the maximum dimension in the projection of the chain on plane:

$$V_e = V(R_M) \quad (32)$$

for linear flexible coil random-flight chains:

$$R_M^2 = \frac{16}{\pi} R_G^2 \quad (33)$$

whereas for a rodlike molecule

$$R_M = L/2 \quad (34)$$

If expressed in terms of R_M , for the random-flight chain (non-draining hydrodynamics)

$$\text{COIL: } M[\eta] = \pi N_A R_M^3 \times 0.18 \quad (35)$$

and for a rodlike molecule

$$\text{ROD: } M[\eta] = \pi N_A R_M^3 \times \frac{1}{3F(L/d_H)} \quad (36)$$

With F put equal to its average value $\langle F \rangle_{\text{AVG}}$ for the range of L/d_H of interest, it is seen that $M[\eta]$ is proportional to R_M^3 for both coil and rodlike chains, so that if Eqn. (32) applies, V_e should be a function of $M[\eta]$ for both chains. For example, if

$$R_M^3 = A' \exp(-BV_e) \quad (37)$$

then

$$M[\eta] = A \exp(-BV_e) \quad (38)$$

where $A = A_c = 0.18 \pi N_A A'$ for coils, and $A = A_R = (1/3 \langle F \rangle) \pi N_A A'$ for rodlike chains. For L/d_H in the range 10 to 100, $\langle F \rangle_{AVG}$ is about 2.5, so that A_R/A_c is about 0.74. As may be seen in the Appendix, the successive ratios M_w/M_n , M_z/M_w , M_{z+1}/M_z calculated from the chromatography data using Eqn. (38) do not depend on A, so that these are expected to be useful so long as V_e can be represented as a function of $M[\eta]$. On the other hand, the averages M_n , M_w , etc., are all proportional to $(A/K)^{\frac{1}{1+a}}$, where $a = \partial \ln [\eta] / \partial \ln M$ and $K = [\eta]/M^a$. Thus, since for rodlike chains, $a \sim 1.8$, neglect of the difference between A_R and A_c could result in the molecular weights based on Eqn. (38) that are about 10 percent too large if V_e is fundamentally a function of R_M .

3. EXPERIMENTAL

1. Absolute Intensity Light Scattering: The Analog Light Scattering Apparatus (ALSA) described previously has been used for all AILS studies described here. As with studies described previously, small Dandliker cells (ca 5 ml solution volume) were used. Solutions were filtered into the cells, degassed and sealed under vacuum to prevent contamination by moisture. Appropriate corrections for absorption and fluorescence were applied. Measurements included $R_{VV}(u)$ or $R_{UV}(u) = R_{VV}(u) + R_{HV}(u)$, and $R_{HV}(u)$. Samples were investigated prior to centrifugation, and after centrifugation in a swinging-bucket rotor (8,000 rpm) for 15-20 hours. In the portion of the cell used for light scattering experiments, the centrifugal field was about 5,000 g.

Evaluation of M_w and $\langle s^2 \rangle^{LS}$ from AILS data requires an estimate for δ . As discussed previously, this can involve comparison of $R_{HV}(u)$ with $R_{VV}(u)$, or can be obtained solely from $R_{HV}(u)$ if the molecules have a rodlike conformation (e.g., small L/ρ).

Thus, for $R_{HV}(u)$

$$\left[\frac{Kc}{R_{HV}(u)} \right]^0 = \frac{5}{3(\delta^2 M)^{LS}} \left[1 + \frac{7}{3} \langle s^2 \rangle_{APP,H} h^2 + \dots \right] \quad (39)$$

where

$$\langle s^2 \rangle_{APP,H} = \frac{f \delta^2 M \langle s^2 \rangle^{LS}}{(\delta^2 M)^{LS}} \quad (40)$$

with the light scattering average Φ^{LS} if a function Φ defined as

$$\Phi^{LS} = \int_0^{\infty} \Phi M f(M) dM / \int_0^{\infty} f(M) dM \quad (41)$$

with $f(M)$ the weight distribution function of M . From Eqn. (39)

$$(\delta^2 M)^{LS} = 5/3 [Kc/R_{Hv}(0)]^0 \quad (42)$$

$$\langle s^2 \rangle_{APP,H} = \frac{7}{3} \frac{1}{[Kc/R_{Hv}(0)]^0} \frac{\partial [Kc/R_{Hv}(u)]^0}{\partial h^2} \quad (43)$$

Although $(\delta^2 M)^{LS}$ and $\langle s^2 \rangle_{APP,H}$ are in general functions of L/ρ , for small L/ρ they become independent of L/ρ :

$$\lim_{L/\rho=0} (\delta^2 M)^{LS} = \delta^2 M_w \quad (44)$$

$$\lim_{L/\rho=0} \langle s^2 \rangle_{APP,H} = \langle s^2 \rangle^{LS} \quad (45)$$

$$\langle s^2 \rangle^{LS} = \frac{1}{12M_w^2} M_w^2 \left(\frac{M_z}{M_w}\right)^2 \frac{M_{z+1}}{M_z} \quad (46)$$

Consequently, if estimates for M_z/M_w and M_{z+1}/M_z are available, the value of $\langle s^2 \rangle_{APP,H}$ can be used to estimate M_w with Eqn. (45). In turn, this value of M_w can be used to estimate δ by use of Eqn. (44).

Given the estimate for δ , data on $R_{Vv}(u)$ or $R_{Uv}(u)$ can be analyzed for M_w and $\langle s^2 \rangle^{LS}$. For example, for small L/ρ ,

$$\left[\frac{Kc}{R_{Uv}(u)} \right]^0 = \frac{1}{(1 + \frac{7}{5} \delta^2) M_w} \left[1 + \frac{1}{3} \langle s^2 \rangle_{APP,H}^2 h^2 + \dots \right] \quad (47)$$

where

$$\langle s^2 \rangle_{\text{APP,H}} = \frac{1 - \frac{4}{5} \delta + \frac{47}{35} \delta^2}{1 + \frac{7}{5} \delta^2} \langle s^2 \rangle^{\text{LS}} \quad (48)$$

with $\langle s^2 \rangle^{\text{LS}}$ given by Eqn. (46). In terms of experimental parameters,

$$\left[\frac{Kc}{R_{Uv}(0)} \right]^0 = \frac{1}{(1 + \frac{7}{5} \delta^2) M_w} \quad (49)$$

and

$$\langle s^2 \rangle_{\text{APP,U}} = \frac{3}{[Kc/R_{Uv}(0)]^0} \frac{\partial [Kc/R_{Uv}(0)]^0}{\partial h^2} \quad (50)$$

For a consistent analysis, M_w and $\langle s^2 \rangle^{\text{LS}}$ obtained with Eqns. (47-50) should be consistent with the values obtained with Eqns. (42-46). Failure for such consistency could involve deviation of the chain conformation from the assumed rodlike structure, or the effects of interchain association. The former should not be a problem unless $L/\rho > 1$.

2. Intensity Fluctuation Light Scattering A Digital Light Scattering Apparatus (DLSA) with a Data Acquisition System (DAS) has been used for IFLS measurements. A schematic drawing of the DLSA is given in Fig. 1. Important experimental parameters include the diameter d of the pinhole, the number of post-autocorrelation average M , and the delay time τ_D used in data collection. In addition, data can be collected with or without the use of a lens to focus the incident

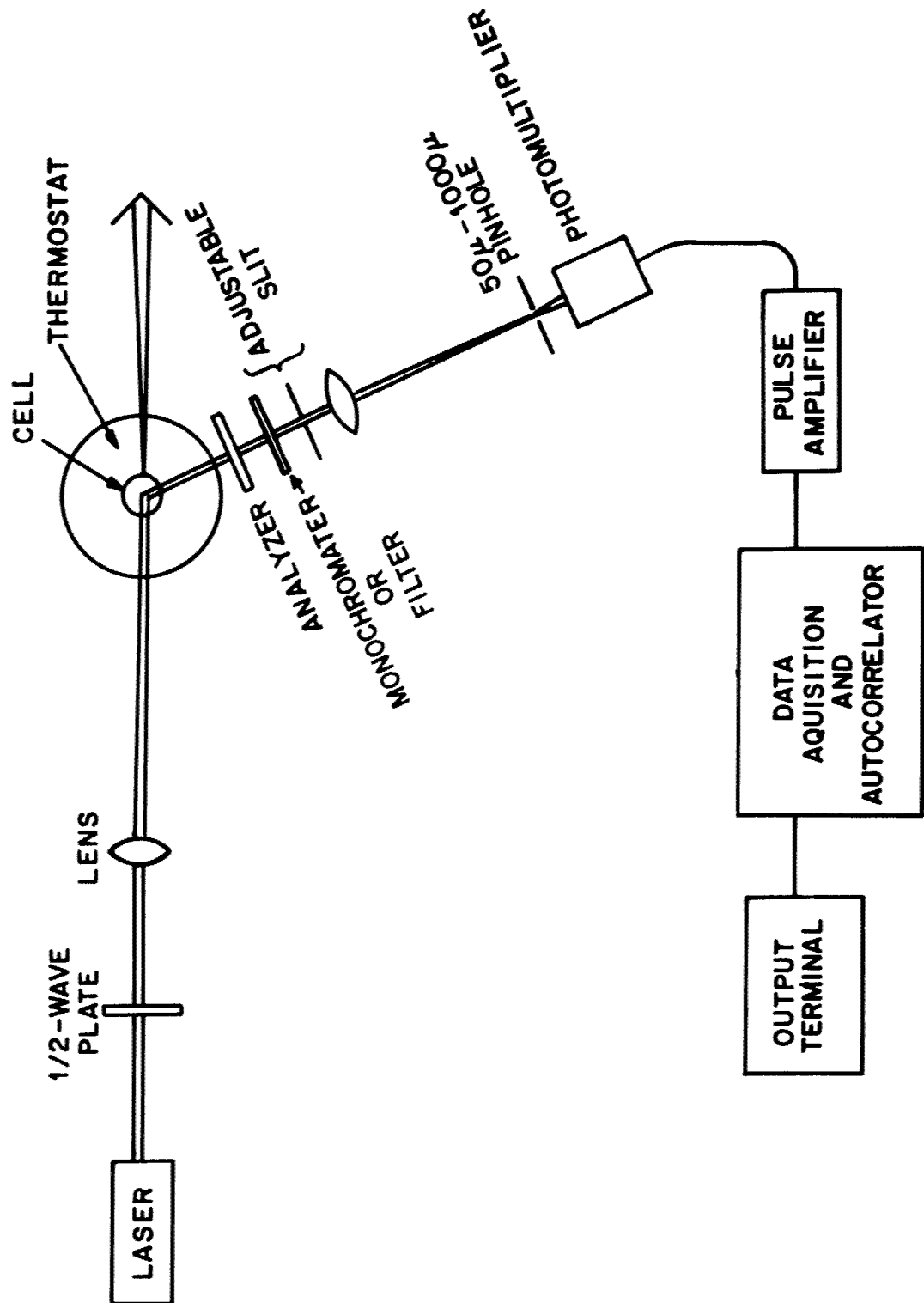


Figure 1 Schematic diagram of IFLS instrument.

beam in the scattering cell. The general relation for the autocorrelation of the scattered light intensity fluctuations can be written in the form

$$\langle n_o n_t \rangle = [\langle n \rangle_{LO} + \langle n \rangle]^2 + 2\langle n \rangle_{LO} \langle n \rangle \gamma' g_1(h, t) + \langle n \rangle^2 [g_2(h, t) - 1] \quad (51)$$

where $\langle n \rangle$ and $\langle n_o n_t \rangle$ are defined above, $\langle n \rangle_{LO}$ is the count rate for a local oscillator mixed with coherence factor γ' with the scattered light, and for the type of scattered light of interest here,

$$g_2(h, t) - 1 = \gamma g_1^2(h, t) = \gamma \exp(-t/\tau_h) \quad (52)$$

For measurements to be considered here, $\langle n \rangle \gg \langle n \rangle_{LO}$, etc., where $\langle n \rangle_{LO}$ arises solely from stray light (dust, reflections, etc.), so that Eqn. (51) reduces to Eqn. (10) given above. In treating IFLS data, it is convenient to analyze the data in terms of the cumulants K_i defined by the relation

$$K_i = -\frac{1}{2} \lim_{t \rightarrow 0} \frac{\partial^i}{\partial t^i} \ln [\langle n_o n_t \rangle - \langle n \rangle^2] \quad (53)$$

Thus, for example,

$$K_1 = D_M h^2 \quad (54)$$

$$K_2 = 0$$

if g_2 is given by Eqn. (11). Deviation of K_2 from zero is an indication of deviation of $g_1(h,t)$ from Eqn. (11b), either because of the effects of molecular weight heterogeneity or intramolecular relaxations.

With the DAS used, t is measured in increments of τ_D :

$$t = \tau_D T \quad (56)$$

where T varies from 1 to 20 and $\tau_D = (12.6 \times 10^{-6})2^N$ (sec) with $N \geq 0$ for the experiments reported here. An argon-ion laser (Lexel Model 85) was used as the light source (in single-mode operation) with an incident intensity of about 0.2 watt at a wavelength of 514.9 nm. This is sufficient to cause localized heating if the beam is focused into dilute solutions of PBO or PBT owing to the weak absorption of light obtained with these polymers. Consequently, it is necessary to use the beam without benefit of focus, resulting in a reduction in the coherence factor γ . The effect of variation of d , M and the use of the lens is illustrated in Fig. 2 which illustrates the autocorrelation function in the form

$$\ln C(T) = \ln \frac{\langle n_0 n_T \rangle - \langle n \rangle^2}{\langle n \rangle^2} \quad (57)$$

obtained for a solution of polystyrene in decalin for a variety of conditions with coherence factors γ ranging from 0.016 to 0.75. It can be seen that satisfactory data can be obtained without the use of a lens, despite the reduction in γ . Moreover, the most efficient

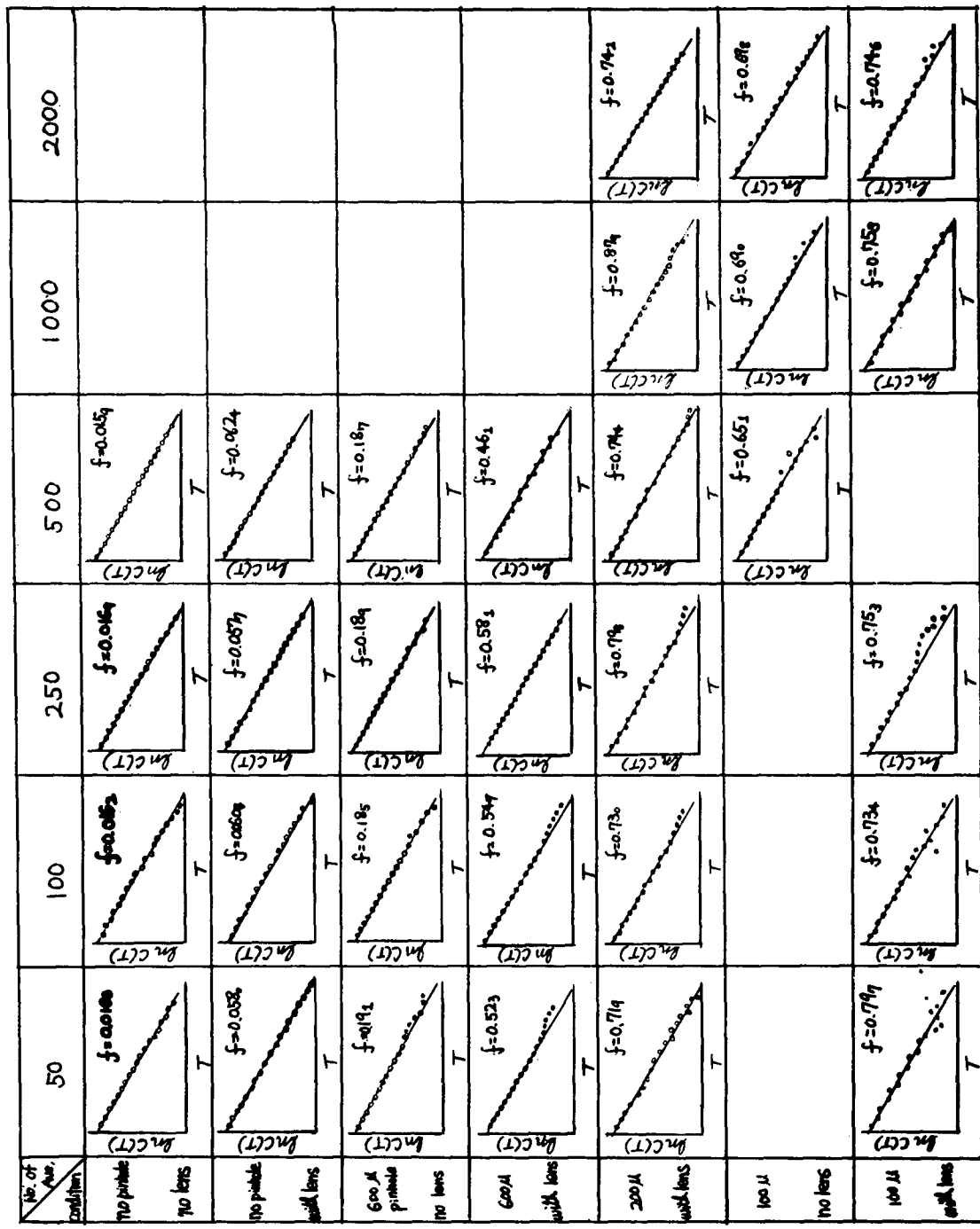


Figure 2 The log of the correlation function and coherence factor f (γ in text) for various combinations of lens, pinhole and number of averages for polystyrene in decalin.

operation (smallest M for satisfactory results) is not obtained with conditions giving the largest γ . Rather, the best range seems to be with γ about 0.1 to 0.2, a range used with most of the experiments on PBO and PBT solutions.

A schematic drawing of the sample cell used for IFLS measurements is given in Fig. 3. The cell requires about 1 ml of solution. With PBO and PBT solutions, the solution was filtered into the cell, degassed and sealed in the cell under vacuum. Solutions were examined both before and after centrifugation, as with AILS measurements. In addition, the IFLS cell holder permits measurements to be made as a function of height in the cell; that is, as a function of position in the centrifugal field experienced during centrifugation.

Even though the solutions of PBO and PBT to be studied absorb some of the 514.5 Å wavelength light, resulting in possible slight localized heating and convection, these effects should not be important so long as $\langle n \rangle_{L0} \ll \langle n \rangle$ (otherwise the term linear in $\langle n \rangle_{L0}$ in Eqn. (51) would contain a factor dependent on the thermal heating effects). In order to confirm the expected behavior, IFLS was measured for solutions of polystyrene in butanone, with and without a small amount of a dye (crystal violet) added to make the absorbance of the polystyrene solution similar to that of the PBO and PBT solutions studied. As may be seen in Fig. 4, the added dye did not affect the IFLS data.

3. Fluorescence Measurements. Measurements of r were made with the ALSA,

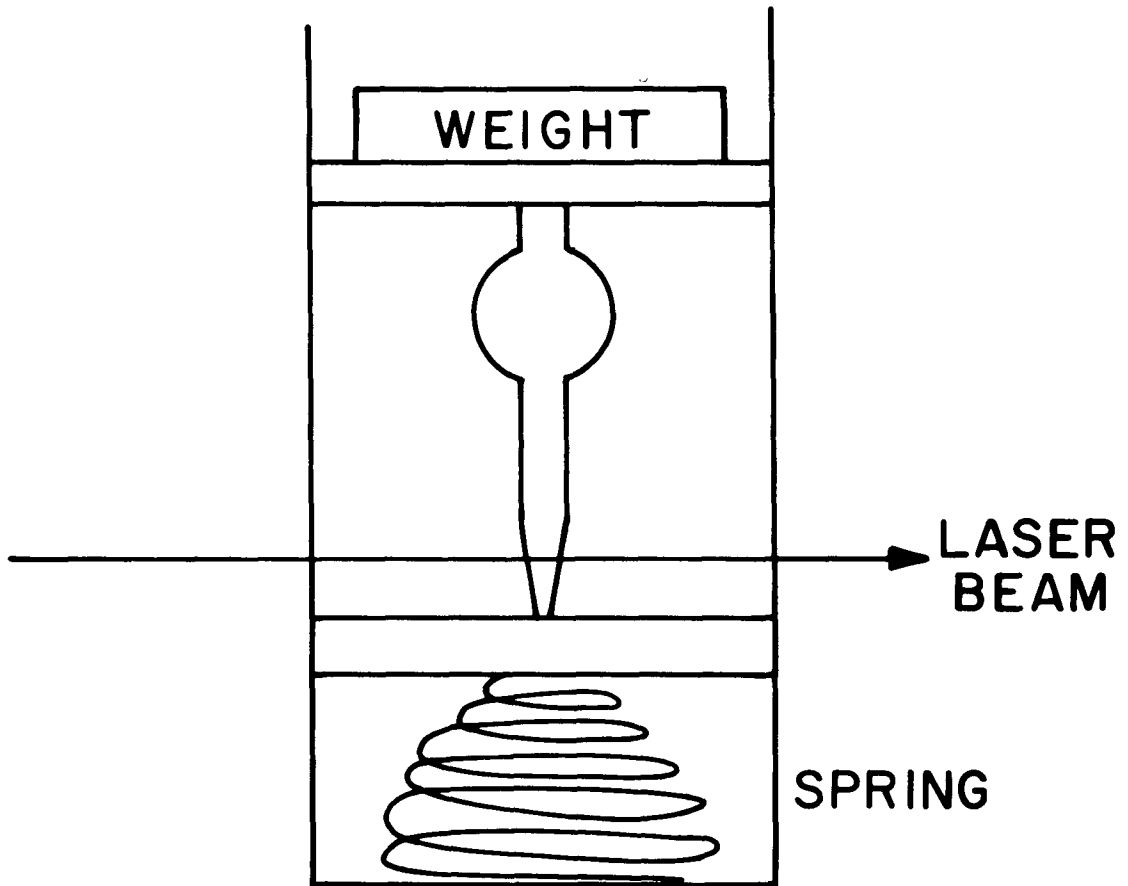


Figure 3 Sample cell used for IFLS measurement allowing adjustment of vertical position.

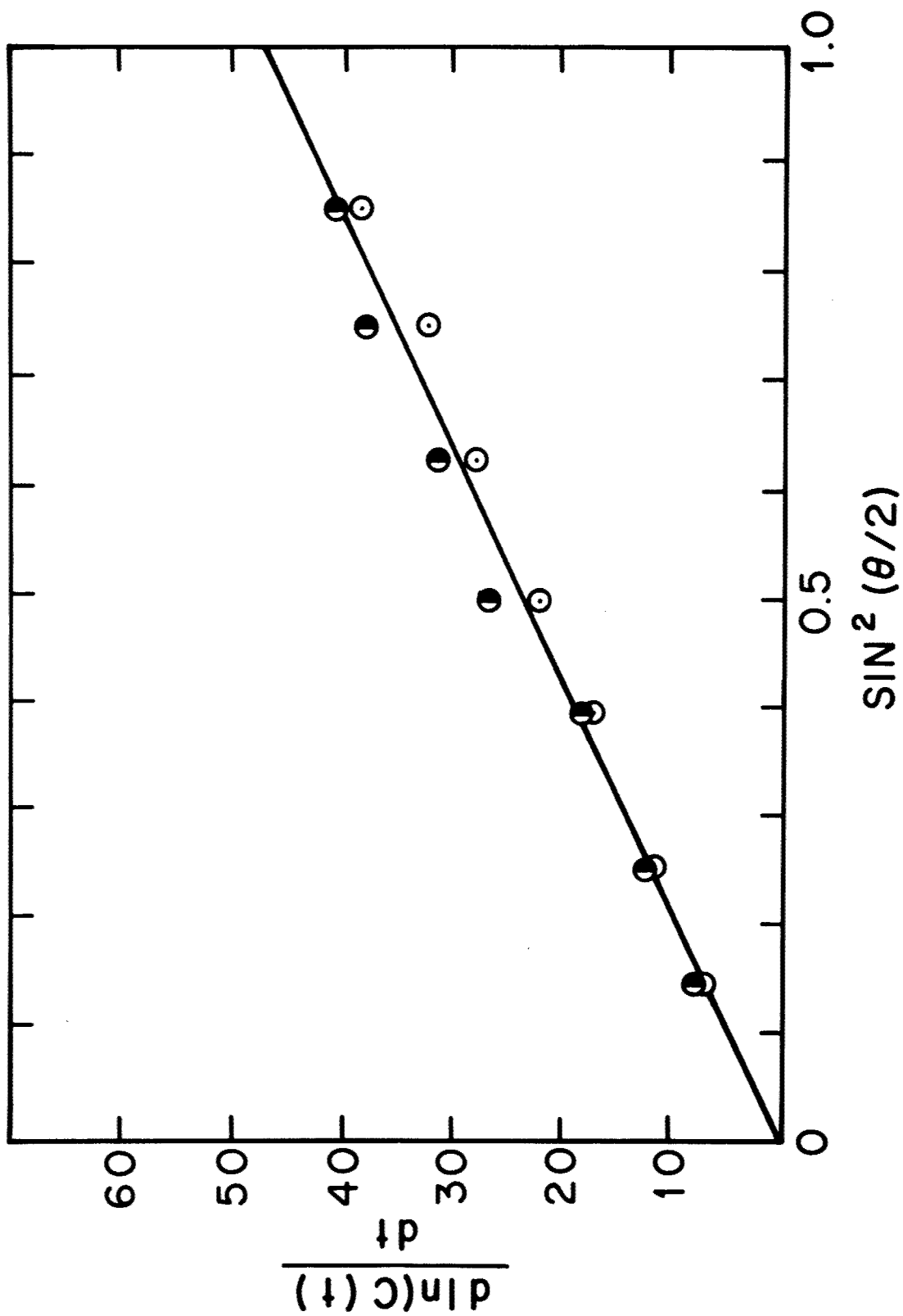


Figure 4 The slope of the log of the correlation function $c(t)$ versus $\sin^2 \theta/2$ for a narrow distribution polystyrene sample in methyl ethyl ketone. Open circles--without added dye. half-filled circles--with added crystal

with 632.8 nm incident radiation from a He-Ne laser, using an interference filter between the sample and the photomultiplier to remove the scattered light at 632.8 nm. Measurements of R^F were made either with the ALSA with 632.8 nm incident radiation or the DLSA with 488.0 or 514.5 nm incident light. In the latter case, a special cell holder was devised to accept a standard 10 mm path length fluorescence cuvette. The holder was equipped to translate the cell along or perpendicular to the incident beam direction by a measurable amount, to permit systematic variation of l and l' (see Eqns. 30 and 31). An interference filter with a variable wavelength along its length was used to select the wavelength λ' of the fluorescence reaching the photomultiplier. With the DLSA, the incident beam was modulated at 450 Hz by a mechanical chopper, so that $C(T)$ is a triangle wave with period $1/450$ s and peak to peak amplitude equal to the square of count rate from the fluorescence intensity. This procedure eliminates the effects of photomultiplier thermionic emission, stray room light, etc., from the count rate used to determine R^F .

With the ALSA, values of R^F are calculated by comparison of the photomultiplier current from the fluorescent sample with that from a glass block with known turbidity. With the DLSA, the count rate from the fluorescent sample was compared to that for the scattering from a polystyrene solution (at the wavelength of the incident light). Thus, values are reported as $R_A^F = R^F/R^S$, where R^S is the Rayleigh ratio of the polystyrene standard.

The response of photomultipliers used in the ALSA and DLSA

is not calibrated as a function of wavelength. Consequently R^F is only known to within a calibration constant equal to the photomultiplier response at λ and λ' .

4. Intrinsic Viscosity. Viscosity measurements were made with suspended-level Ubbelohde viscometers using methods described previously. Solutions were filtered into the viscometers and maintained under nitrogen during measurements. Owing to the long flow times used, kinetic energy corrections to the flow time were negligible, so that the relative viscosity $\eta_{rel} = \eta/\eta_s$ was just the ratio of solution and solvent flow time. Graphical representation of the data included plots of $\eta_{sp}/c = (\eta_{rel} - 1)/c$, $(\ln \eta_{rel})/c$ and $[\eta]_c \equiv [2(\eta_{sp} - \ln \eta_{rel})]^{1/2}/c$ versus c , according to the relations:

$$\frac{\eta_{sp}}{c} = [\eta]\{1 + k'[\eta]c + k''([\eta]c)^2 + \dots\} \quad (58)$$

$$\frac{\ln \eta_{rel}}{c} = [\eta]\{1 - (\frac{1}{2} - k')[\eta]c + (\frac{1}{3} - k' + k'')([\eta]c)^2 + \dots\} \quad (59)$$

$$[\eta]_c = [\eta]\{1 - (\frac{1}{3} - k')[\eta]c + \dots\} \quad (60)$$

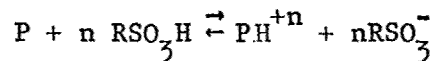
For typical flexible chain polymers, $(\frac{1}{3} - k')[\eta]c \ll 1$ for concentrations used, so that $[\eta]_c \approx [\eta]$.

5. Exclusion Chromatography. An exclusion chromatograph described elsewhere was used to study solutions of PBO and PBT in methane sulfonic acid (MSA). The column was calibrated to give the elution volume V_e as a function of $M[\eta]$ for flexible chain polymers, and has been used

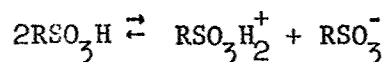
with heterocyclic polymers in MSA. A visible absorption spectrometer was used to determine the eluent concentrations as a function of V_e .

4. RESULTS AND DISCUSSION

4.1 The Effects of Ionic Strength: In previous reports, it has been shown that PBO and PBT are protonated in acids of the type RSO_3H .



In addition, the protic sulfonic acids are self-protonated in varying degree to produce ions that alter the ionic strength I:



Owing to long range intermolecular electrostatic interactions, the ionic strength of the acid solvent can have considerable effect on properties such as η_{sp}/c (or $[\eta]_c$), A_2^{LS} and Ξ_c^{LS} (the latter at concentration c). In particular, the ionic strength is very low for ClSO_3H ($I \sim 10^{-3}$ mol/l), whereas it is rather large for $\text{CH}_3\text{SO}_3\text{H}$ ($I \sim 5 \times 10^{-2}$ mol/l), two of the solvents most often used with PBO and PBT. With these two reagents, the Debye ionic radius b^{-1} , calculated as

$$b^2 = \frac{8\pi N_A e^2}{1000 \epsilon kT} I \quad (61)$$

is 3 Å for $\text{CH}_3\text{SO}_3\text{H}$, but 50 Å for ClSO_3H (with the dielectric constant ϵ equal to 100).

The effect of this difference on A_2^{LS} may be seen in Fig. 5, showing results for $Kc/R_{UV}(0)$ and $Kc/R_{HV}(0)$ for solutions of a PBT

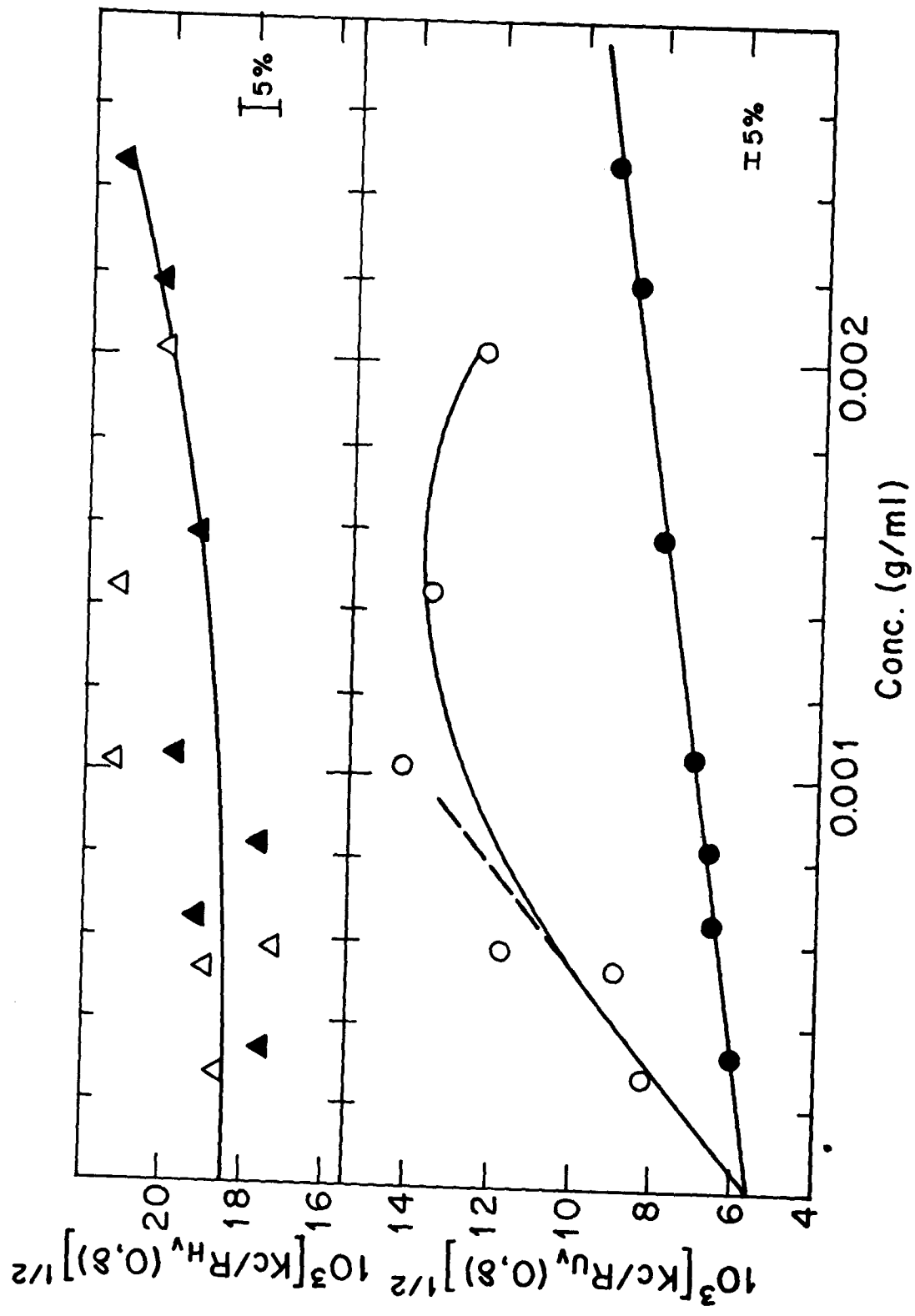


Figure 5 Light scattering data on PBT-2G in methanesulfonic acid (filled symbols) and chlorosulfonic acid (unfilled symbols).

polymer in both $\text{CH}_3\text{SO}_3\text{H}$ and ClSO_3H . With both solutions, $\partial[\text{Kc}/\text{R}_{\text{HV}}(0)]/\partial c$ is about zero, as expected with Eqn. (9). For the solutions in $\text{CH}_3\text{SO}_3\text{H}$, the data give $M_w A_2^{\text{LS}} = 400 \text{ ml/g}$, or if $A_2^{\text{LS}} \sim A_2^{\text{L}}$ for the rodlike chain, a thermodynamic diameter $d_H = 3 \text{ \AA}$ for PBT in $\text{CH}_3\text{SO}_3\text{H}$. It may be noted that $d_H \sim b^{-1}$ in this case. By contrast, with the solutions in ClSO_3H , A_2^{LS} is so large that reliable extrapolation to give $[\text{Kc}/\text{R}_{\text{UV}}(0)]^0$ is prohibited. On the other hand, since $[\text{Kc}/\text{R}_{\text{HV}}(0)]^0$ is equivalent in both solvents, it is reasonable to estimate A_2^{LS} by extrapolation of the data in ClSO_3H solution to the value $[\text{Kc}/\text{R}_{\text{UV}}(0)]^0$ found with the $\text{CH}_3\text{SO}_3\text{H}$ solution. If this is done, then the estimate $M_w A_2^{\text{LS}} = 2000 \text{ ml/g}$ is found, or $d_H = 13 \text{ \AA}$ for PBT in ClSO_3H , in comparison with $b^{-1} = 50 \text{ \AA}$ for ClSO_3H . By contrast with d_H values of $\langle s^2 \rangle^{\text{LS}}$ determined from $\langle s^2 \rangle_{\text{APP},\text{H}}$ are essentially the same in the two solvents. Evidently, the intermolecular electrostatic interactions can become extremely large if I is small enough.

A similar result is observed with hydrodynamic data. For the concentration range usually studied, values of η_{sp}/c (or $[\eta]_c$) are much larger for solutions of PBO in ClSO_3H in comparison with $\text{CH}_3\text{SO}_3\text{H}$. In fact, some typical data are shown in Fig. 6. It can be seen that for solutions with concentration c such that $c[\eta] > ca 0.04$, η_{sp}/c is much larger in ClSO_3H than in $\text{CH}_3\text{SO}_3\text{H}$, with η_{sp}/c exhibiting a pronounced downward curvature for smaller c . It appears that data in both solvents will give the same value of $[\eta]$, as would be expected if d_H is the same, for the polymer in the two solvents at infinite dilution. Curiously, for solutions with $c[\eta] > 0.04$, it appears that $[\eta]_c^{-1}$ is

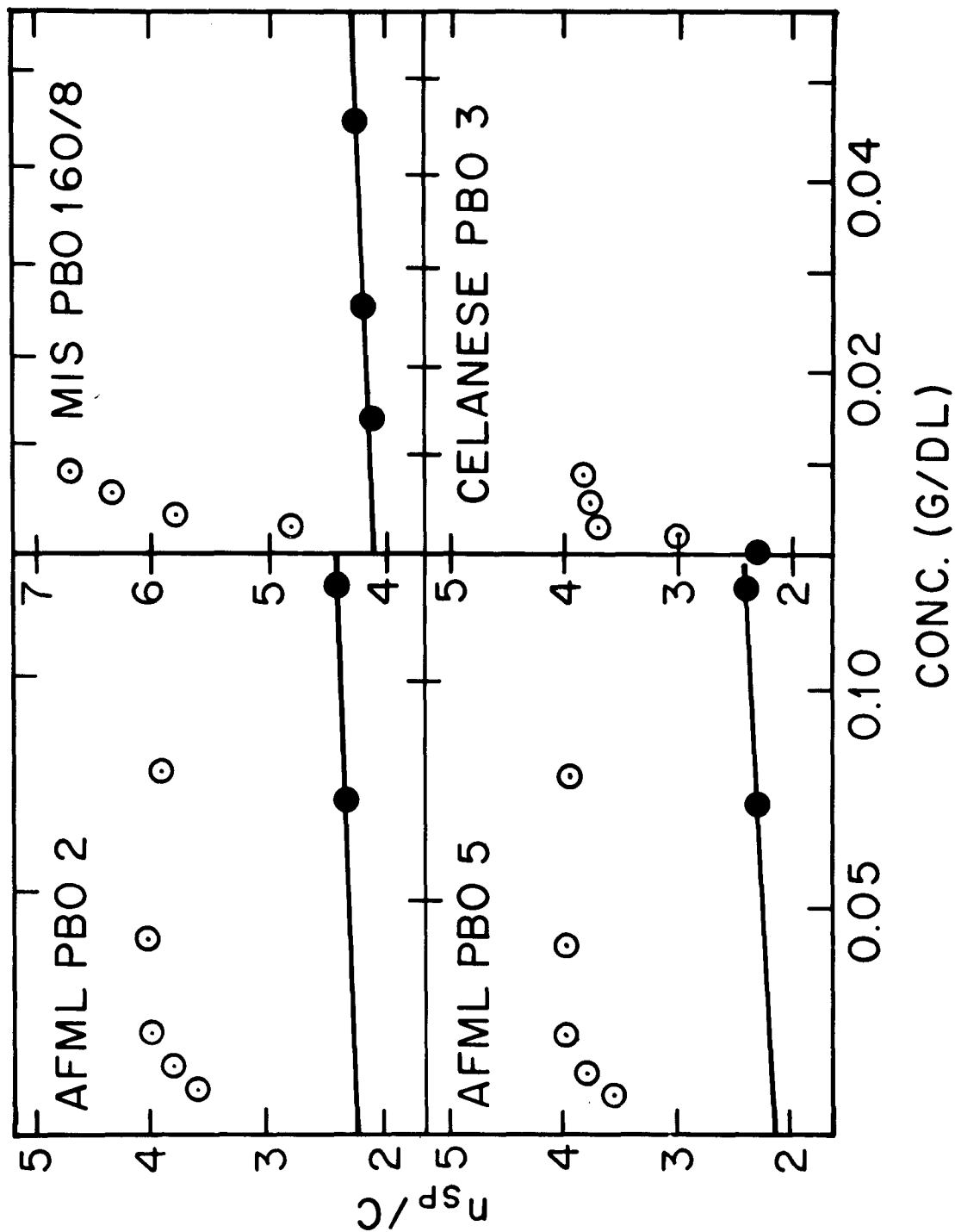


Figure 6 η_{sp}/c versus concentration for four PBO polymers in methanesulfonic acid (filled symbols) and chlorosulfonic acid (unfilled symbols).

nearly inversely proportional to \sqrt{c} , with $m = \partial[\eta]_c^{-1} / \partial c^{1/2}$ nearly the same (0.2) for several PBO polymers with $[\eta] \sim 2.3$, but with m tending to decrease to zero for PBO polymers with smaller $[\eta]$. In general, it appears that m is smaller with PBT polymers in comparison with PBO solutions.

The observation that η_{sp}/c appears to decrease sharply for $c[\eta] < ca\ 0.04$ suggests that the effects of the long range repulsive interactions decrease sharply as c is decreased below this level. If the solute concentration is expressed as an apparent volume fraction φ_A defined as

$$\varphi_A = v \frac{4\pi}{3} \left(\frac{L}{2}\right)^3 \quad (62)$$

where $v = Mc/N_A$ is the number of chains per unit volume, then the apparent volume fraction φ_A^* corresponding to the condition $c[\eta] = 0.04$ is given by

$$\varphi_A^* = 8F \times 0.04 \quad (63)$$

with F given by Eqn. (5c). For L/d_H in the range of interest here, this result gives $\varphi_A^* \sim 0.5$, showing that the packing of the 'equivalent spheres' swept out by rotation of the rodlike chains is quite dense for $c[\eta] \sim 0.04$. Apparently, with solutions of PBO in low ionic strength solvents, the electrostatic interactions are sufficient to result in near mutual exclusion of chains from the molecular volume

swept out by a rod in rotatory motion about its center. With solvents with a higher ionic strength, these interactions are effectively shielded, so that, for example, $[\eta]_c$ is nearly independent of c as expected for polymers with only short range repulsive interactions.

The variation of $[\eta]_c$ with c for $c[\eta] > 0.04$ may reflect to a slight increase in the shielding of electrostatic interactions with increasing c . Such an effect might reasonably have $[\eta]_c^{-1}$ proportional to $c^{1/2}$.

The hydrodynamic data obtained by IFLS exhibit a parallel behavior. Values of $D_M \eta_s$ determined for a PBO polymer in solutions in $\text{CH}_3\text{SO}_3\text{H}$, ClSO_3H or ClSO_3H containing 0.01 M ClSO_3Li are shown in Fig. 7. It is seen that in pure ClSO_3H , D_M is about 100 fold smaller than in $\text{CH}_3\text{SO}_3\text{H}$, or in ClSO_3H containing added salt. According to Eqn. 13-15,

$$D_M \approx \frac{kT}{\Xi^0} \frac{(1 + 2A_2Mc + \dots)}{(1 + f(M, A_2)c + \dots)} \quad (64)$$

It may be seen that the observed effects of long-range electrostatic interactions are not predicted by Eqn. (64), unless $f(M, A_2)$ is much greater than A_2M . A large $f(M, A_2)$ is unusual, but would be consistent with the very large $\partial[\eta]_c / \partial c$ observed with PBO solutions in ClSO_3H .

The small values of D_M for solutions in ClSO_3H indicates that molecular translation is nearly prohibited by long range electrostatic interactions. In principle, the emission anisotropy r can be used to study the effects of ionic strength on the rotatory diffusion constant D_R by use of Eqns. (25-29). In practice, for PBO and PBT,

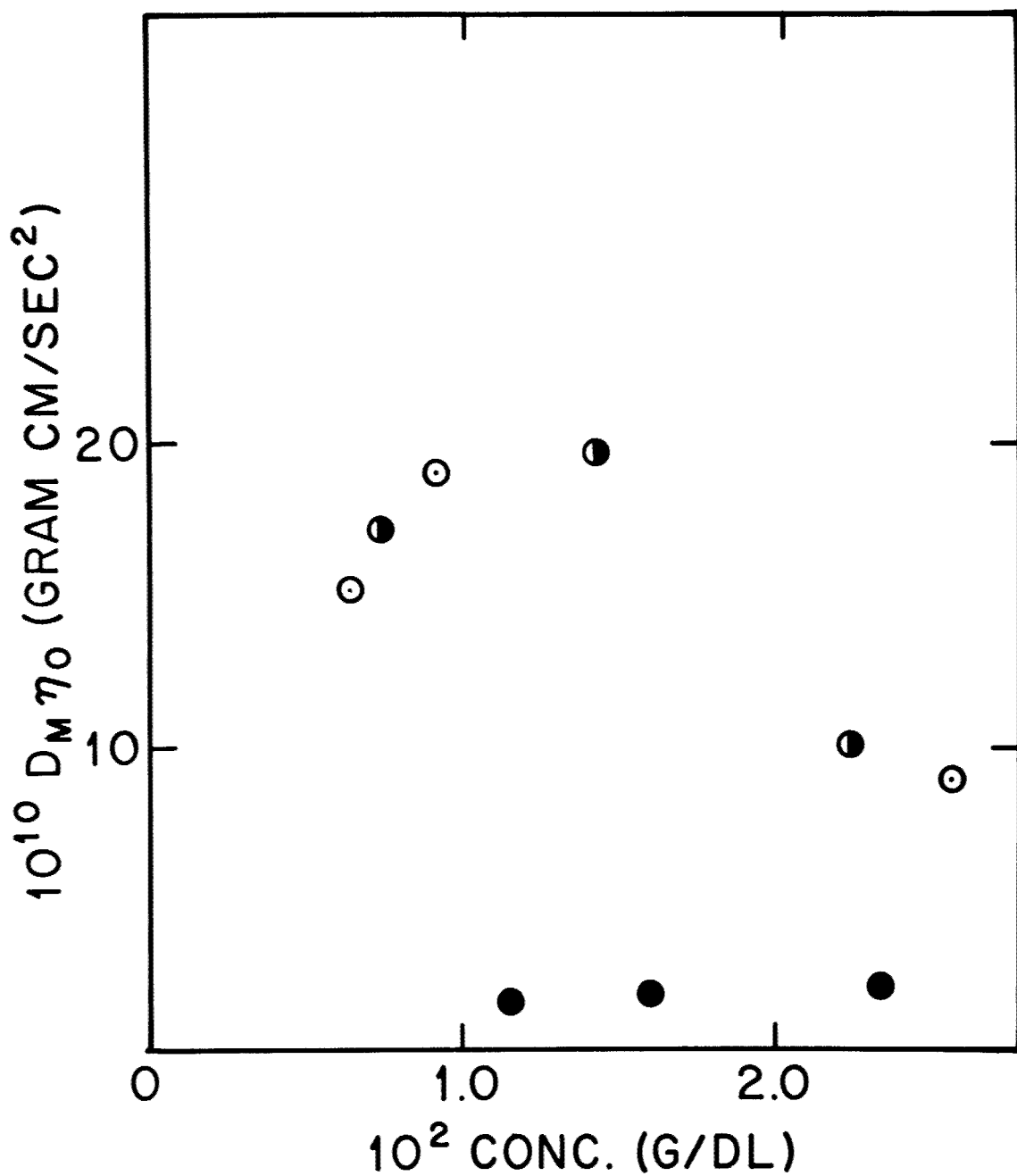


Figure 7 $D_M \eta_0$ for CMU PBO 160/8 in methane sulfonic acid (unfilled symbols), chlorosulfonic acid (filled symbols) and chlorosulfonic acid with added lithium chlorosulfonate (half-filled symbols).

values of r are usually in the range 0.2 to 0.34, and are influenced considerably by low molecular weight components of the molecular weight distribution (see Eqn. 29). Excitation lifetime measurements (obtained with the cooperation of Dr. Kohji Chihara, CMU Department of Chemistry) show that τ_E is in the range 1.5×10^{-9} s for PBO, so that if $\beta = 0$ ($r_0 = 0.4$), then D_R^F is in the range 10^8 sec^{-1} , so that chains with M in the range 1000 and less contribute greatly to D_R^F . With Eqns. 25-29, the quantity $D_R^F \eta_s$ is given by

$$6\tau_E(D_R^F \eta_s) = \eta_s(r_0 - r)/r \quad (65)$$

Therefore, effects of ionic strength on rotatory diffusion should be revealed as variations of $\eta_s(r_0 - r)/r$. Values of η_s are 2.5 cp for ClSO_3H and 10.5 for $\text{CH}_3\text{SO}_3\text{H}$ at 25°C . Typically, values of r are nearly the same for solutions of a particular PBO or PBT polymer in ClSO_3H and $\text{CH}_3\text{SO}_3\text{H}$, despite the substantial difference in the viscosity of these two solvents. Consequently, either $\tau_E D_R^F$ is so small that $r \sim r_0 < 0.4$ or D_R^F is significantly less in ClSO_3H than in $\text{CH}_3\text{SO}_3\text{H}$. Studies on concentrated isotropic solutions (ca 2 percent) give $r \sim r_0$ equal to 0.4.

This suggests that D_R^F is, in fact, depressed in a low ionic strength solution, as is D_M .

2. Exclusion Chromatography. Exclusion chromatography obtained for several polymers in $\text{CH}_3\text{SO}_3\text{H}$ are shown in Figs. 8 and 9. The chromatography reveal considerable difference in the molecular weight distribution of the polymers studied. Values of M_w/M_n , M_z/M_w , etc. were

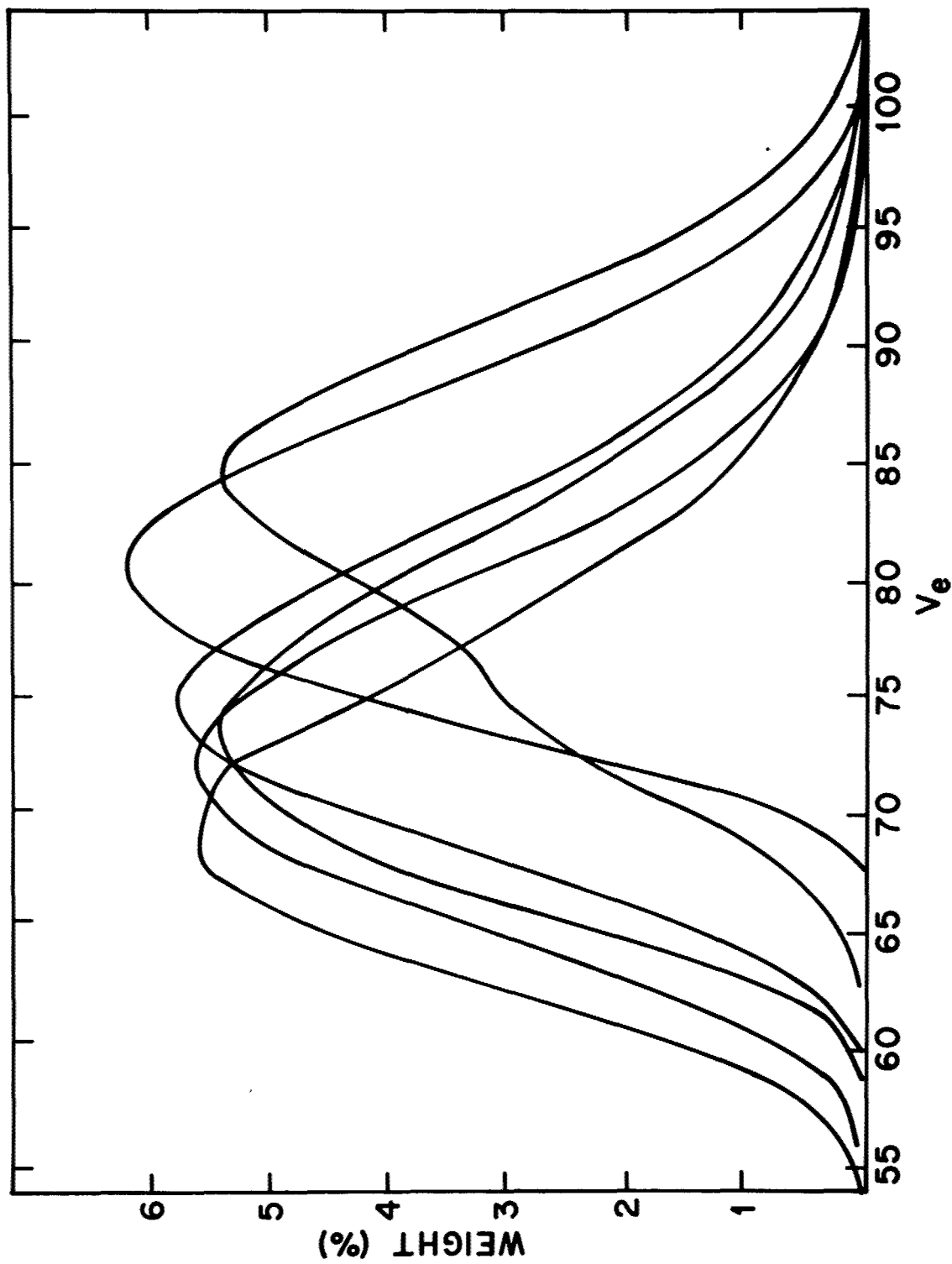


Figure 8 Exclusion chromatography obtained on several PBO polymers in MSA. Left to right: CMU 160/8, Celanese 9A, AFML 2, AFML 5, Celanese 3, and AFML 6.

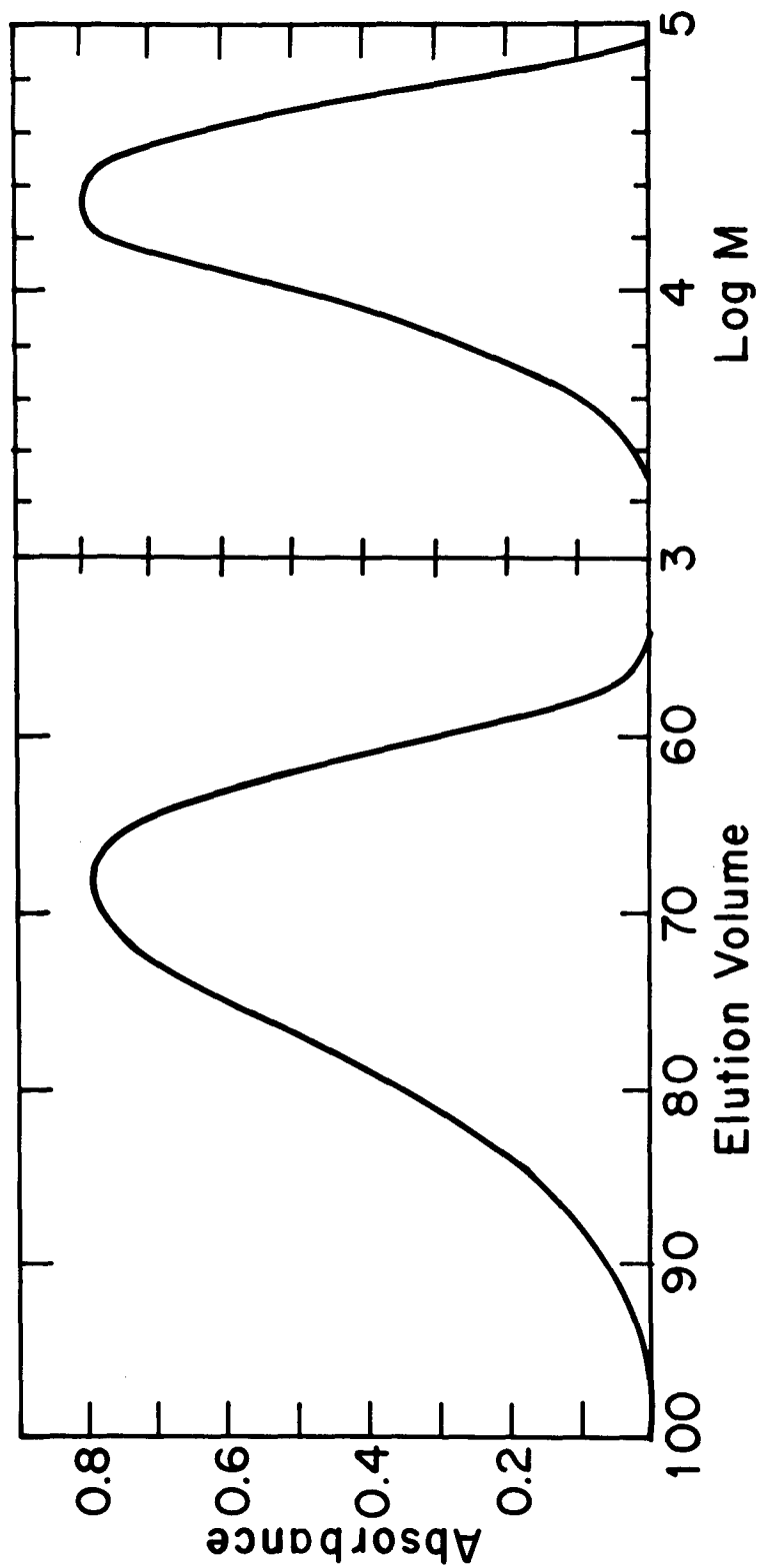


Figure 9 Exclusion chromatography obtained for SRI PBI 20. Absorption of the eluent at 440 nm versus elution volume V_e and $\log M$.

calculated with Eqn. (38), using the constant B established by calibration with flexible chain polymers, and Eqn. (1A) from the Appendix. For example, $M_w/M_n = M_1/M_0$, with $f(V_e)$ equal to the (relative) concentration of the solution with elution volume V_e . As shown above, the constant A is not needed to compute M_w/M_n , etc. The exponent $a = \partial \ln[\eta] / \partial \ln M$ was put equal to 1.8 in the calculations. Values of M_w/M_n , etc. are entered in Table 1, along with M_e , calculated as

$$M_e[\eta] = \Sigma w_j (M[\eta])_j \quad (66)$$

where w_j is the fraction of the eluent with elution volume $(V_e)_j$ within dV_e , and $(M[\eta])_j$ is computed with Eqn. (38). Estimation of M_e does require use of the coefficient A. In these calculations, it is assumed that $A = A_c$, the value established with a flexible chain polymer. If Eqn. (37) should be applied instead, then, as mentioned above, values of M deduced with Eqn. (38) using $A = A_c$ instead of $A = A_R$ will be about 10 percent too large.

The values of M_w/M_n , etc. are surprisingly small for a step-growth polymer. This effect has been discussed elsewhere¹⁵ in terms of the polymerization mechanism with the rodlike chain.

3. Fluorescence and Absorption. The electronic absorption spectra of two PBO polymers are shown in Fig. 10. It may be seen that the extinction coefficient μ is identical for the two polymers for short wavelengths, but that substantial differences between the spectra obtain in the long wavelength region. This behavior is characteristic

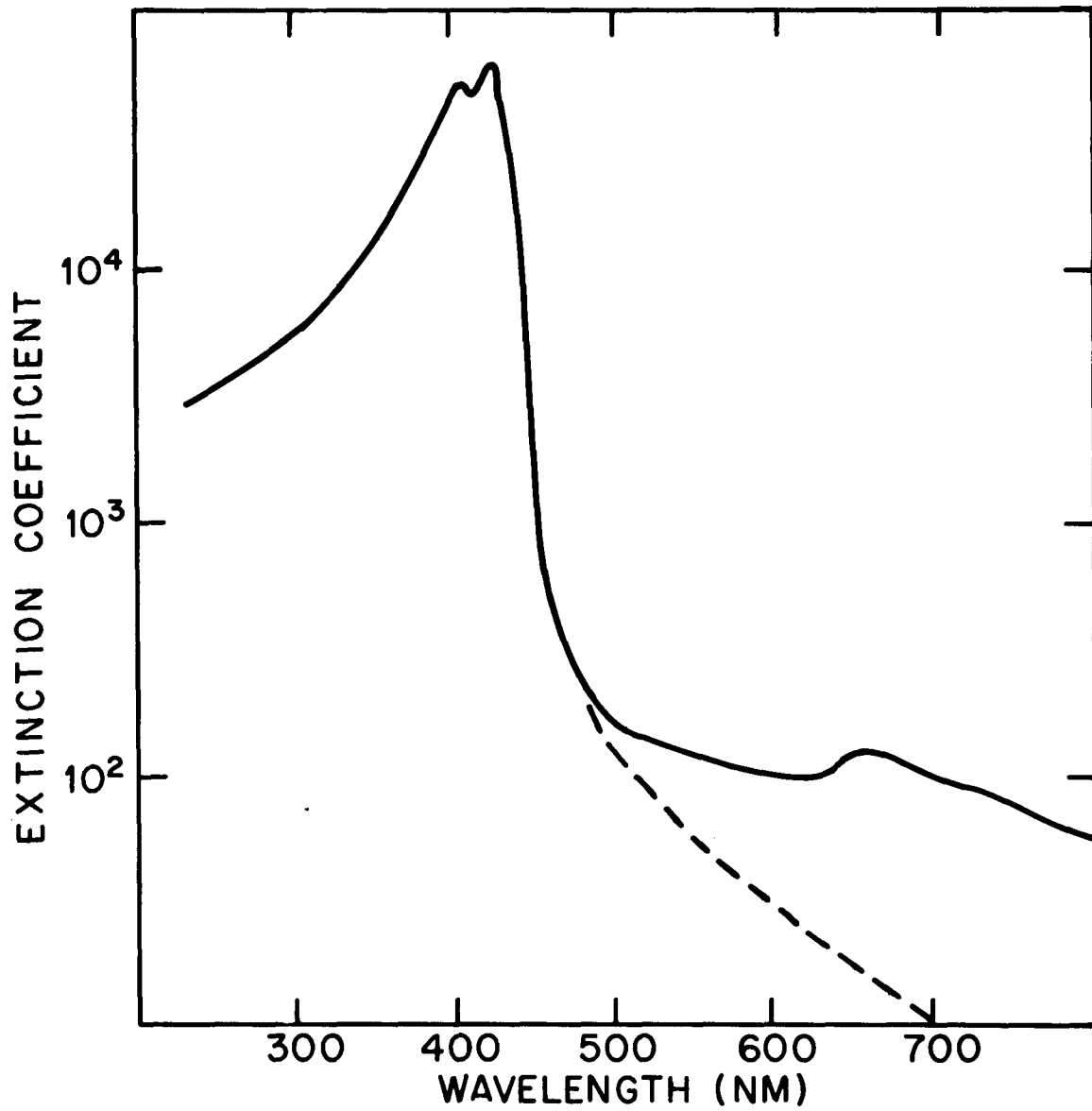


Figure 10 Absorption spectra of AFML PBO-5 (solid line) and CMU PBO 160/8 (dashed line) showing differences at long wavelengths.

TABLE 1

EXCLUSION CHROMATOGRAPHY DATA OBTAINED ON
SEVERAL PBO POLYMERS; ORIGINAL AND AFTER
PRECIPITATION FROM METHANE SULFONIC ACID SOLUTION

Polymer	M_e	M_w/M_n	M_z/M_w	M_z/M_{z+1}
MIS-160/8	17,000	1.60	1.49	1.38
1st recov.	15,500	1.53	1.47	1.40
AFML-2	11,000	1.49	1.38	1.29
1st recov.	12,300	1.52	1.45	1.36
AFML-6	6,000	1.45	1.46	1.39
AFML-5	10,000	1.44	1.37	1.30
Cel. -3	6,200	1.28	1.23	1.18
Cel. -9A	14,000	1.50	1.45	1.37

of the spectra for all of the PBO polymers examined. The spectra for the long wavelength region for several PBO polymers is shown in Fig. 11. It appears that some of the polymers have a component with substantial absorption in the long wavelength region, but it does not appear that all of the data can be entirely explained by postulating various compositions of two components. The long wavelength spectra of a series of PBO polymers removed from a polymerization flask after various times of polymerization are shown in Fig. 12. It can be seen that the shorter chain length polymers obtained early in the polymerization exhibit the strongest long wavelength absorption. For these polymers, the trend is regular, and the observed spectra can be understood as the sum of the spectra for two components, one with very weak absorption in the long wavelength region and one with strong absorption and two absorption maxima in the shorter wavelength region--both have the same absorption in the short wavelength region. Tentatively, we suggest that the characteristic strong long wavelength absorption is due to undissolved, small microcrystalline PBO fragments. For example, the characteristic green color of solutions with strong long wavelength absorption is similar to that for concentrated solutions of PBO in HOSO_3H which are known to contain undissolved PBO. Moreover, it seems reasonable to associate absorption at such long wavelengths with some form of a strongly interacting solute structure. Since the extinction coefficient for the postulated second component is unknown at present, we cannot estimate the fraction that might be present from the observed extinction, but it is believed to be

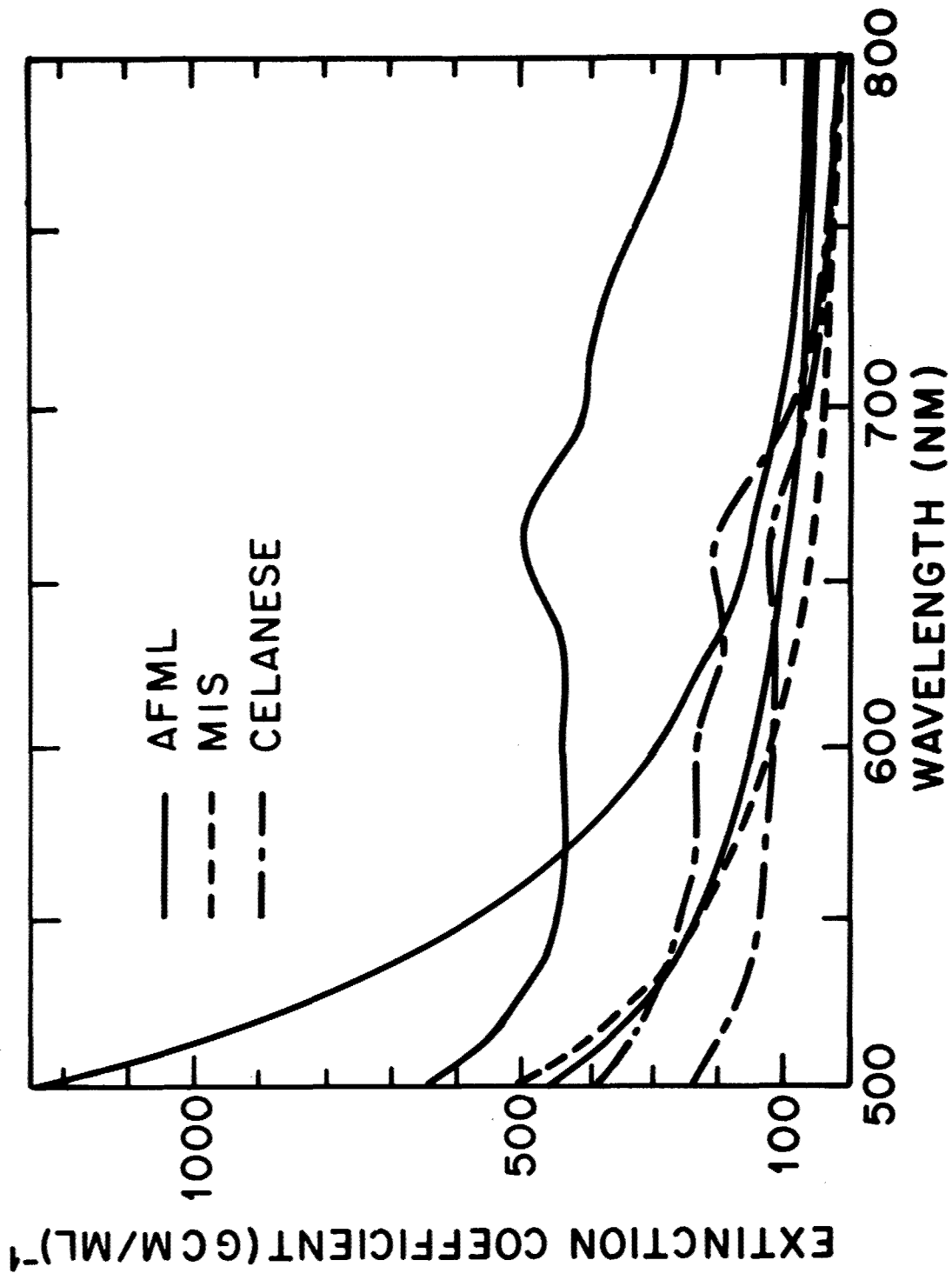


Figure 11 Absorption spectra of several PBO polymers in the long wavelength region.

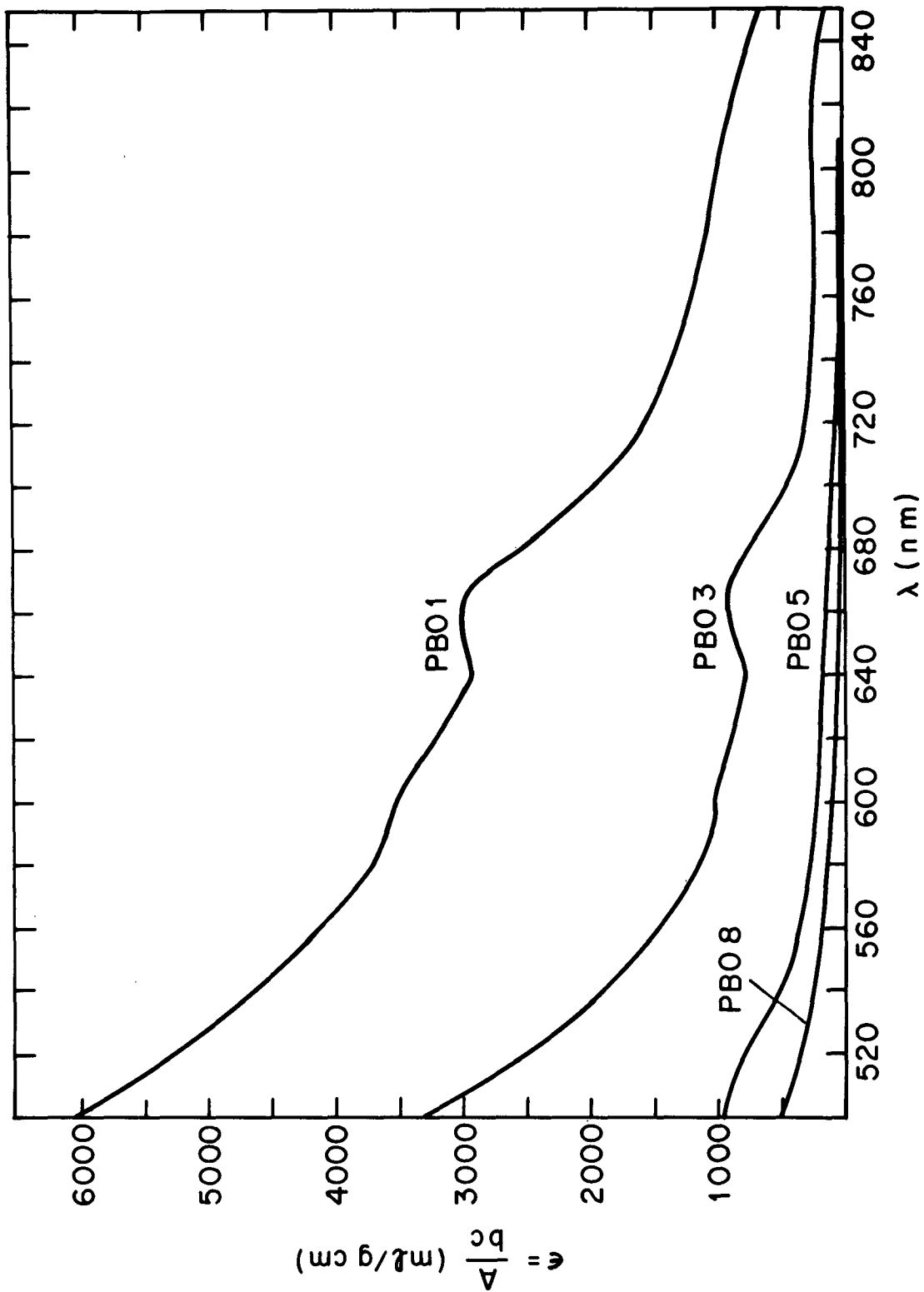


Figure 12 Absorption spectra at long wavelength for a series of aliquots removed from a polymerization in PPA at 160°C.

only a small amount or involve very small aggregates since the material is not evident on visual inspection.

The fluorescence spectra of PBO is as complex as the absorption spectra. The (uncorrected) spectra observed with a low molecular weight PBO MIS-160/4 (absorption spectra in Fig. 12) for several excitation wavelength are given in Fig. 13. Three separate emission bands may be identified: one emission is excited by absorption in the low wavelength region (400 to 500 nm); a second is excited in the midrange of the absorption spectra (500 to 600 nm); and a third is excited by absorption in the red wavelength range (greater than 600 nm). Absorption at 514.5 nm excites both of the latter. The data shown in Fig. 13 were obtained with the DLSA using reflected optics (R_B^F).

Some data for $\ln(R_P^F/c)$ as a function of c for PBO, MIS-160/1 and MIS-160/3 (see absorption spectra in Fig. 12) in $\text{CH}_3\text{SO}_3\text{H}$ are shown in Fig. 14. In these experiments, $\lambda = 514.5$ nm and $\lambda' = 686$ nm. According to Eqn. (30b), the intercepts at infinite dilution give $\mu_{\lambda} K_A^0$ and the slopes give $\mu_{\lambda} l + \mu_{\lambda'} l' + K_q$. (The quantum efficiency is an apparent value since the wavelength dependence of the photomultiplier is unknown). Since $\mu_{\lambda} l$ and $\mu_{\lambda'} l'$ are precisely known, the latter gives the Perrin quenching coefficient K_q . The results,

	μ_{664}	$\mu_{514.5}$	$\mu_{514.5} K_A^0$	K_A^0	K_q
MIS 160/1	2.9	1.22	1.95	1.60	0.41
MIS 160/3	0.9	0.62	0.56	0.90	0.42

show that K_A^0 calculated as $\mu_{514.5} K_A^0$ divided by $\mu_{514.5}$ is not the same

* The subscript A indicates an apparent K^0 from relative intensities.

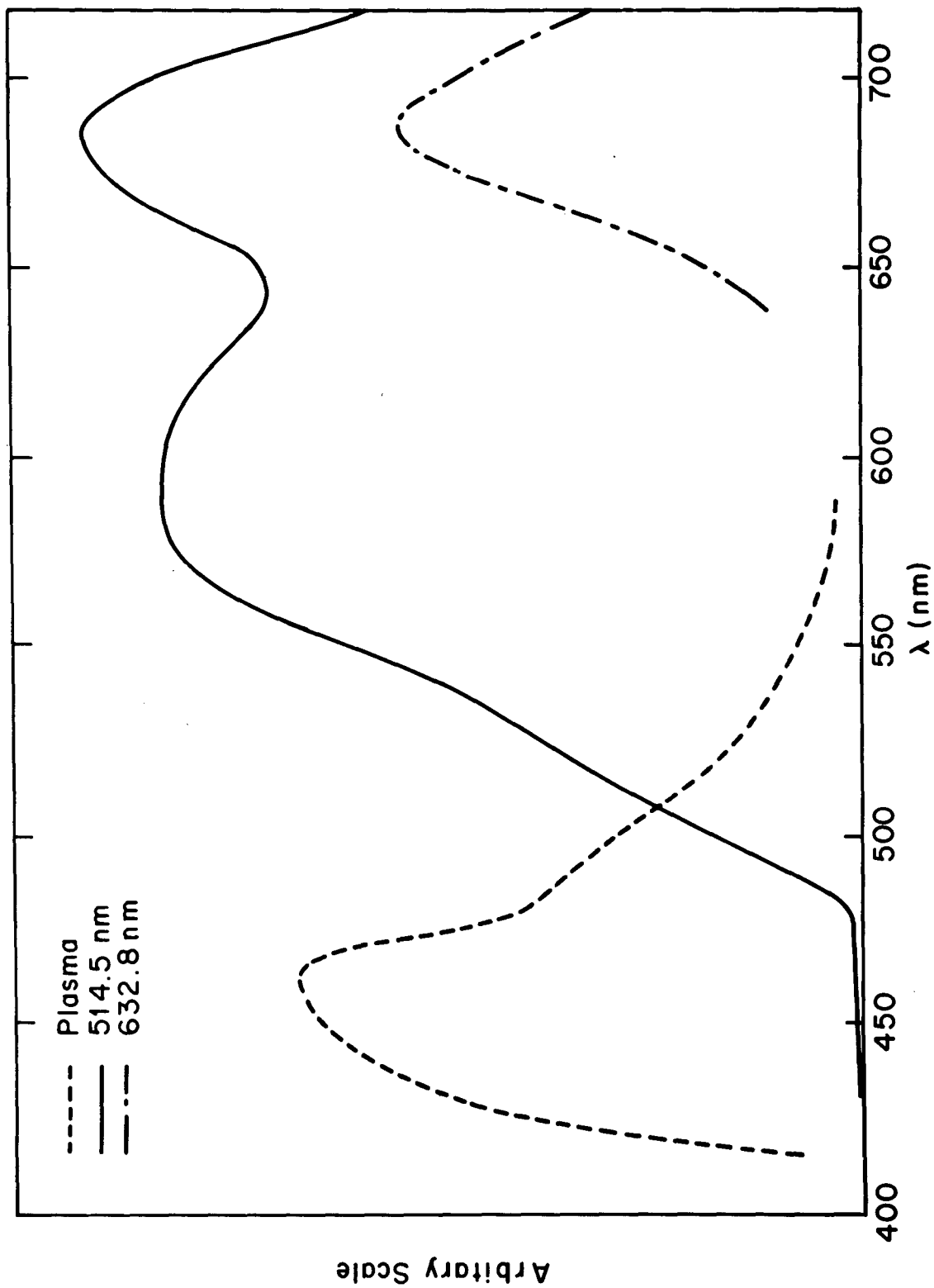


Figure 13 Fluorescence emission spectra obtained for CMU PBO 160/4 in methane sulfonic acid with excitation at the wavelengths indicated.

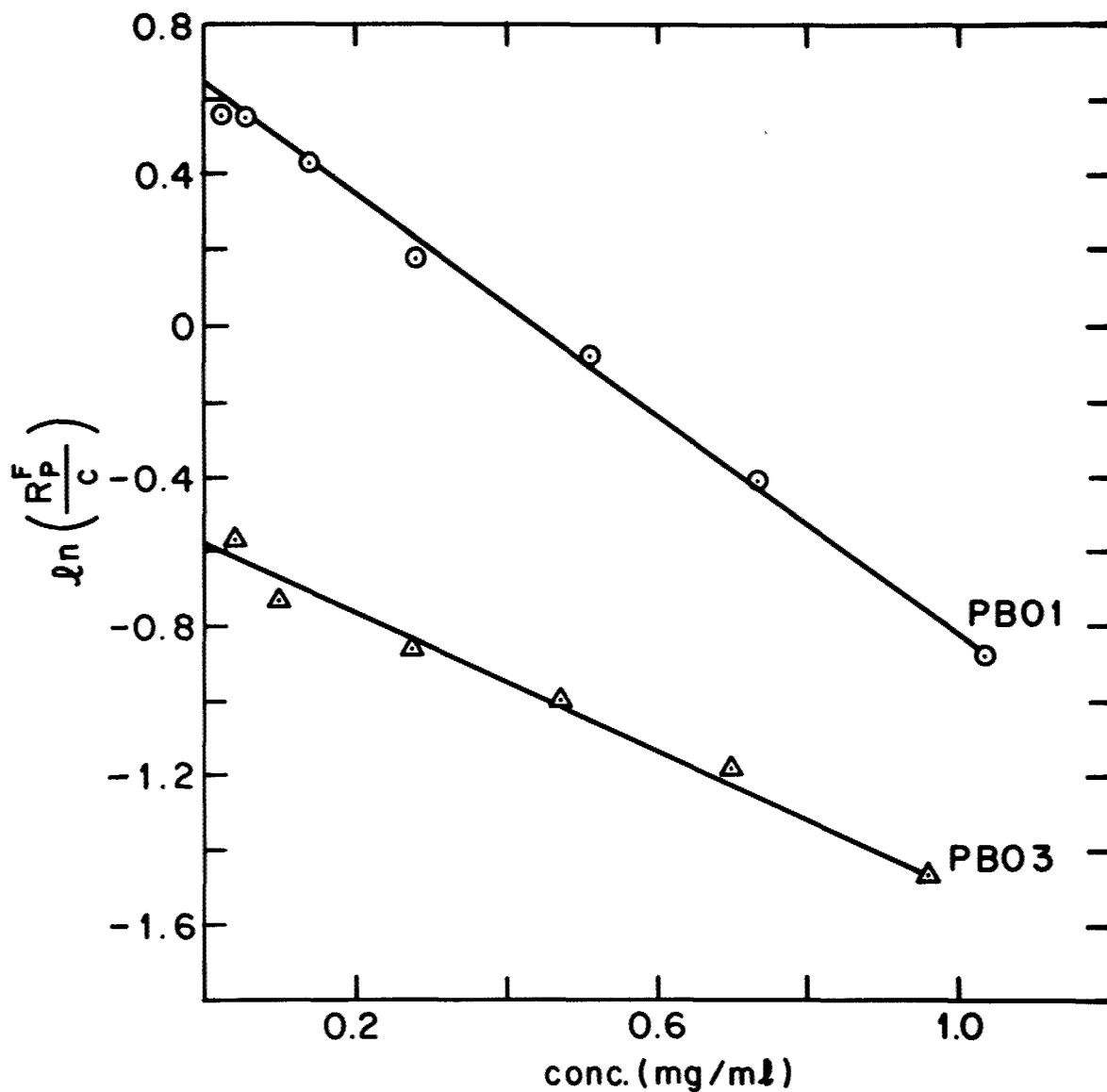


Figure 14 $\ln(R_p^F/c)$ versus concentration in methane sulfonic acid (see Eqn. 36 in text) for two early aliquots removed from a polymerization in PPA at 160°C. Excitation at 514.5 nm, emission at 686 nm.

for the two PBO polymers, whereas K_q is constant. It is possible that the true quantum yield for the fluorescent species with emission maxima at 686 nm should be the same for the two polymers, and that the apparent difference in K_A^0 reflects the effects of some absorption at $\mu_{514.5}$ giving rise to species that do not give fluorescence at 686 nm. (That this is true is evident, for example, in Fig. 13). For example, if the absorption at 664 nm is characteristic only of the fluorescent species, then $\mu_{\lambda} K_A^0 / \mu_{664}$ would be expected to be more constant than K_A^0 itself. For the data on MIS 160/1 and 3, this ratio is nearly constant at 0.65. With this simple interpretation, variation of K_A^0 calculated by division of $\mu_{\lambda} K_A^0$ by μ_{λ} provides information on the extent of aggregation.

Additional data have been collected on R_p^F/c for a number of PBO and PBT polymers using the ALSA with 632.8 nm incident wavelength. As seen in Fig. 13. fluorescence emission centered at 686 nm is excited by 632.8 nm incident light. With the ALSA, an interference filter was used to reject 632.8 nm light, but accept light of other wavelengths. Thus, Eqn. (30b) becomes

$$R_p^F/c = \mu_{\lambda} K^0 \sum_{\lambda'} f(\lambda') \exp[-(\mu_{\lambda} l + \mu_{\lambda', l'} + K_q) c] \quad (67)$$

where $f(\lambda')$ is the transmission factor of the interference filter for light of wavelength λ' ; $f(\lambda')$ is a relatively flat function with the interference filter used. With the arrangement used, $l = l' \sim 6$ mm. Plots of $\ln R_p^F/c$ versus c are shown in Fig. 15 & 16 for PBO and Fig. 17 for PBT polymers. The solvent fluorescence has been subtracted from

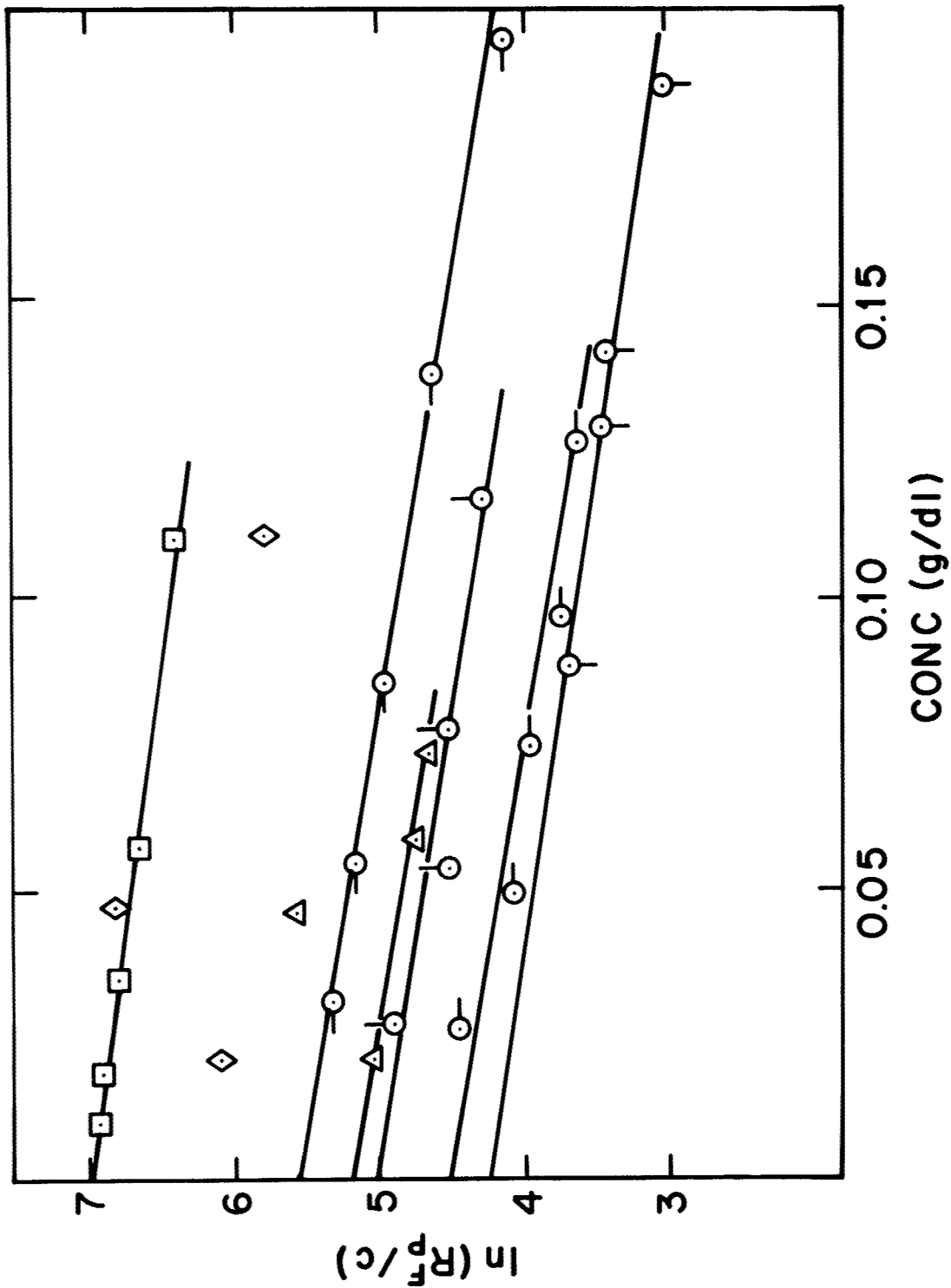


Figure 15 $\ln(R_p^F/c)$ versus concentration for several PBO polymers in chlorosulfonic acid. Excitation at 632.8 nm. Circles with pips clockwise from top: AFML PBO 30, AFML PBO 9, AFML PBO 2, and AFML PBO 6. Triangles: CMU PBO 160/8; squares: Celanese PBO 3 and diamonds: Celanese PBO 9A.

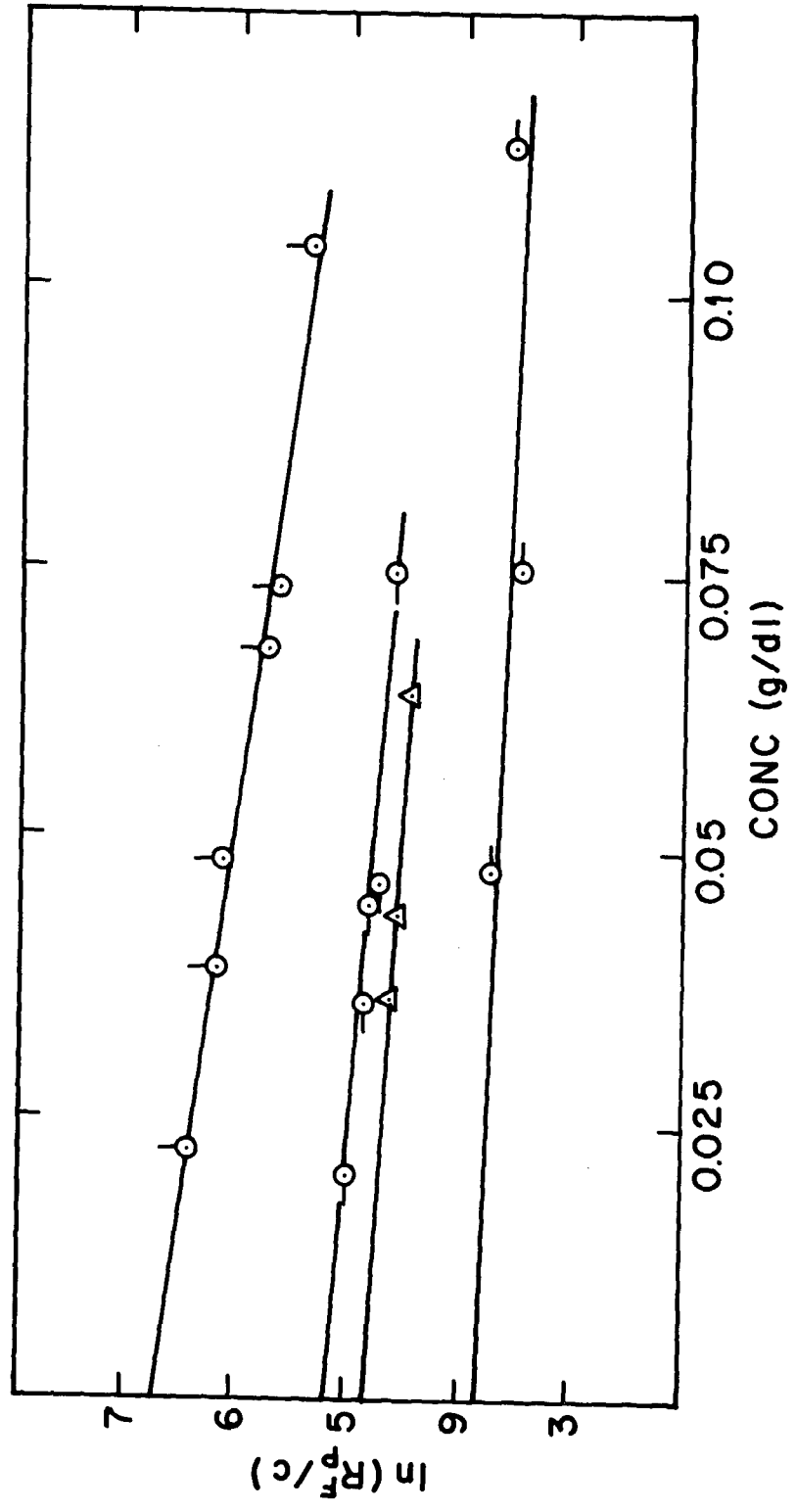


Figure 16 $\ln(R_p^F/c)$ versus concentration for several PBO polymers in methane sulfonic acid. Excitation at 632.8 nm. Circles with pips clockwise from left: AFML PBO 6, AFML PBO 5 and AFML PBO 9. Triangles: CMU PBO 160/8.

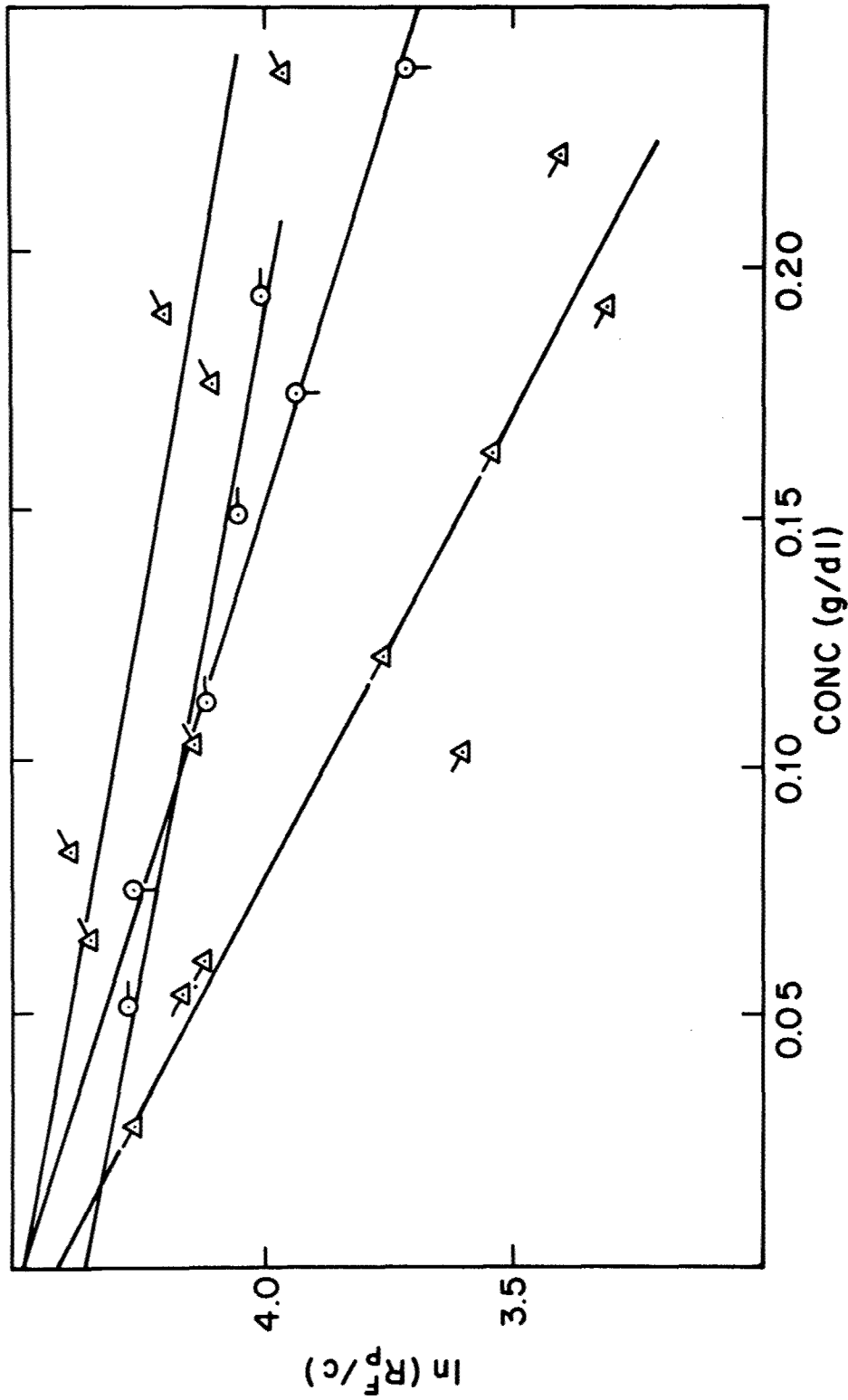


Figure 17 $\ln(R_p/c)$ versus concentration for two PBT polymers. Excitation at 632.8 nm. Triangles: SRI PBT 20; pips left: chlorosulfonic acid, pips right, methane sulfonic acid. Circles: SRI PBT 23; pips down: chlorosulfonic acid; pips right: methane sulfonic acid.

the total for the data shown in Figs. 14-17. Satisfactory linear plots of R_p^F versus c are obtained, showing Eqn. (67) can be approximated as

$$\ln R_p^F/c = \ln \mu_\lambda K_A^0 - (\mu_\lambda \ell + \mu_{EFF} \ell + K_q)c \quad (68)$$

where μ_{EFF} is an effective extinction coefficient for the fluorescent radiation. Values of $\mu_{632.8}$, $\mu_\lambda K_A^0$ and K_A^0 are entered in Table 2 for several polymers in CH_3SO_3H and $ClSO_3H$. Considerable variation of $\mu_{632.8}$ is seen among the polymers, reflecting the variations among the spectra shown in Fig. 11.

The data in Table 2 exhibit a complex relation between μ_λ and $\mu_\lambda K_A^0$. By contrast, as may be seen in Fig. 14-17, the tangent $\partial(\ln R_p^F/c)/\partial c$ is nearly the same for all the PBO polymers studied, with the factor $(\mu_\lambda + \mu_{EFF})\ell + K_q$ in Eqn. (68) about equal to 700 ± 100 ml/g, or $K_q = 700 - \ell(\mu_\lambda + \mu_{EFF})$. Since $\mu_\lambda \sim \mu_{EFF} \sim 350$ ml/g cm for most of the polymers studied, this result (with $\ell = 0.7$ cm) gives $K_q \sim 200$ ml/g. With PBO AFML-5, μ_λ is about 985 ml/g cm, and $(\mu_\lambda + \mu_{EFF})\ell + K_q$ is 1360 ml/g. These data will also give $K_q \sim 200$ ml/g if μ_{EFF} is about 670 ml/g cm. These estimates are a little less than the more precise value $K_q = 410$ ml/g given above for data on low molecular weight PBO polymers. Nevertheless, it appears that with both estimates the long wave fluorescence from PBO is seen to exhibit intermolecular quenching of the Perrin type.

Centrifugation of dilute PBO solutions usually results in

TABLE 2

Extinction Coefficient $\mu_{632.8}$; and K_A^0 From
Intercepts of Figures 15 and 16

	<u>CSA</u>			<u>MSA</u>		
	$\mu_{632.8}$	$\mu_{632.8} K_A^0$	K_A^0	$\mu_{632.8}$	$\mu_{632.8} K_A^0$	K_A^0
AFML-5	1150	-	-	985	880	0.9
AFML-6	560	250	0.45	360	170	0.5
CEL -3	470	1100	2.35	440	-	-
AFML-2	430	74	0.17	265	-	-
AFML-9	290	95	0.3	345	60	0.17
CEL -94	280	665	2.4	250	-	-
MIS -60/8	240	170	0.7	345	140	0.4
AFML-30	200	160	0.8	-	-	-

a small increase in R_p^F at high total solute concentration, and a decrease (few percent) in R_p^F at low solute concentration. If the solution contains two components (designated as 1 and 2) then (for $l = l'$)

$$\frac{\partial \ln R_p^F}{\partial c_1} = \frac{\mu_{\lambda,1} K_1 c_1}{\mu_{\lambda,1} K_1 c_1 + \mu_{\lambda,2} K_2 c_2} - (\mu_{\lambda,1} + \mu_{\lambda',1}) l \quad (69)$$

Consequently, the observed increase in R_p^F could correspond to a decrease in the concentration c_1 of some component present in small amount that is strongly absorbing, but not too fluorescent. If it is assumed that $c = c_1 + c_2 \sim c_2$, and that $c_2/c_1 \sim \text{constant}$, then $\partial \ln R_p^F / \partial c$, will be negative (increase in R_p^F) at large c if $(\mu_{\lambda,1} + \mu_{\lambda',1}) l$ is large enough. As c decreases, the positive term on the rhs of Eqn. (69) will eventually dominate, and $\partial \ln R_p^F / \partial c$, will become positive.

As shown in Table 2, neither $\mu_{\lambda} K_A^0$ or K_A^0 are constants for all of the PBO polymers examined. Some samples (e.g., CEL-3, CEL-9A and AFML-5) give substantially greater fluorescence than the remaining PBO polymers, and to an extent, μ_{λ} is also large for these polymers, albeit that K_A^0 is itself on the high side. Apparently, with these polymers, the data can be understood by postulating the presence of an absorbant, fluorescent species of PBO, possibly a microcrystalline phase. These are the polymers for which the long wavelength absorption spectra exhibits a peak at 664 nm (see Fig. 11). Polymers AFML-2 and 9 give the lowest value of $\mu_{\lambda} K_A^0$ (~ 80), even though μ_{λ} is rather large for AFML-2. These may contain small, variable amounts of some aggregated PBO. With polymers AFML-6 and 30 and MIS-160/8, $\mu_{\lambda} K_A^0$

tends to be larger than the minimal value (e.g. 160-250 instead of 80), again with μ_λ variable. These polymers may contain both of the postulated minor components in varying degree.

4.4 Effects of Centrifugation: It was mentioned above that the fluorescence behavior is affected by centrifugation, apparently by the removal of some strongly absorbing minor component. The angular dependence of the light scattering studied by AILS also reveals the loss of some minor component after centrifugation. Plots of $\ln R_{Vv}$ versus h^2 exhibit decreased initial slope $\partial \ln R_{Vv} / \partial h^2$ and decreased intercept $R_{Vv}(0)$ after centrifugation. Typical data are shown in Figs. 18 and 19. Both effects can be attributed to the removal of a fairly large, minor component during centrifugation. The apparent radius of gyration $\langle s^2 \rangle_{APP}$ equal to $(1/3) \partial \ln R_{Vv} / \partial h^2$ is about $5 \times 10^6 \text{ \AA}^2$.

Interestingly, $R_{Hv}(h)$ is usually not greatly changed by centrifugation, see Figs. 18 and 19. Apparently, the minor, relatively large component that has an appreciable effect on $R_{Vv}(h)$ does not affect $R_{Hv}(h)$ in so disproportionate a fashion. This may indicate that the minor component consists of a disorganized aggregation of the rodlike chains.

The cells used for IFLS experiments permit measurements at several heights along the cell length, corresponding to different positions in the centrifugal field when the cell was centrifuged in a swinging-bucket rotor. Owing to the small diameter of the cell, redistribution of species separated during centrifugation is slow.

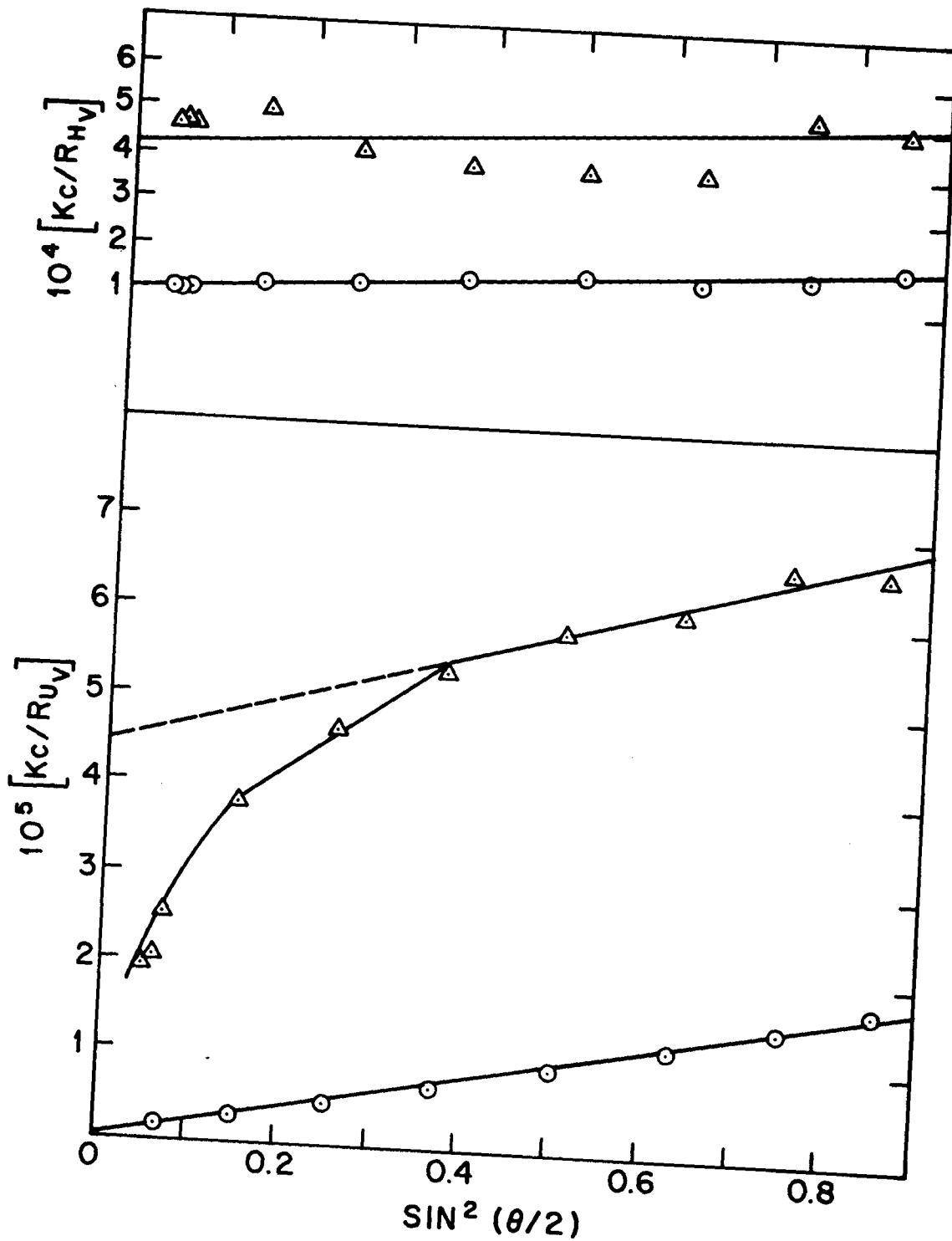


Figure 18 Reciprocal total scattering (U_V) and depolarized scattering (H_V) from vertically polarized incident beam for CMU PBO 160/8 in methane sulfonic acid.* Circles: uncentrifuged triangles: after centrifugation 16 hours at 5,000 G. $c = 0.045 \text{ g/dl}$

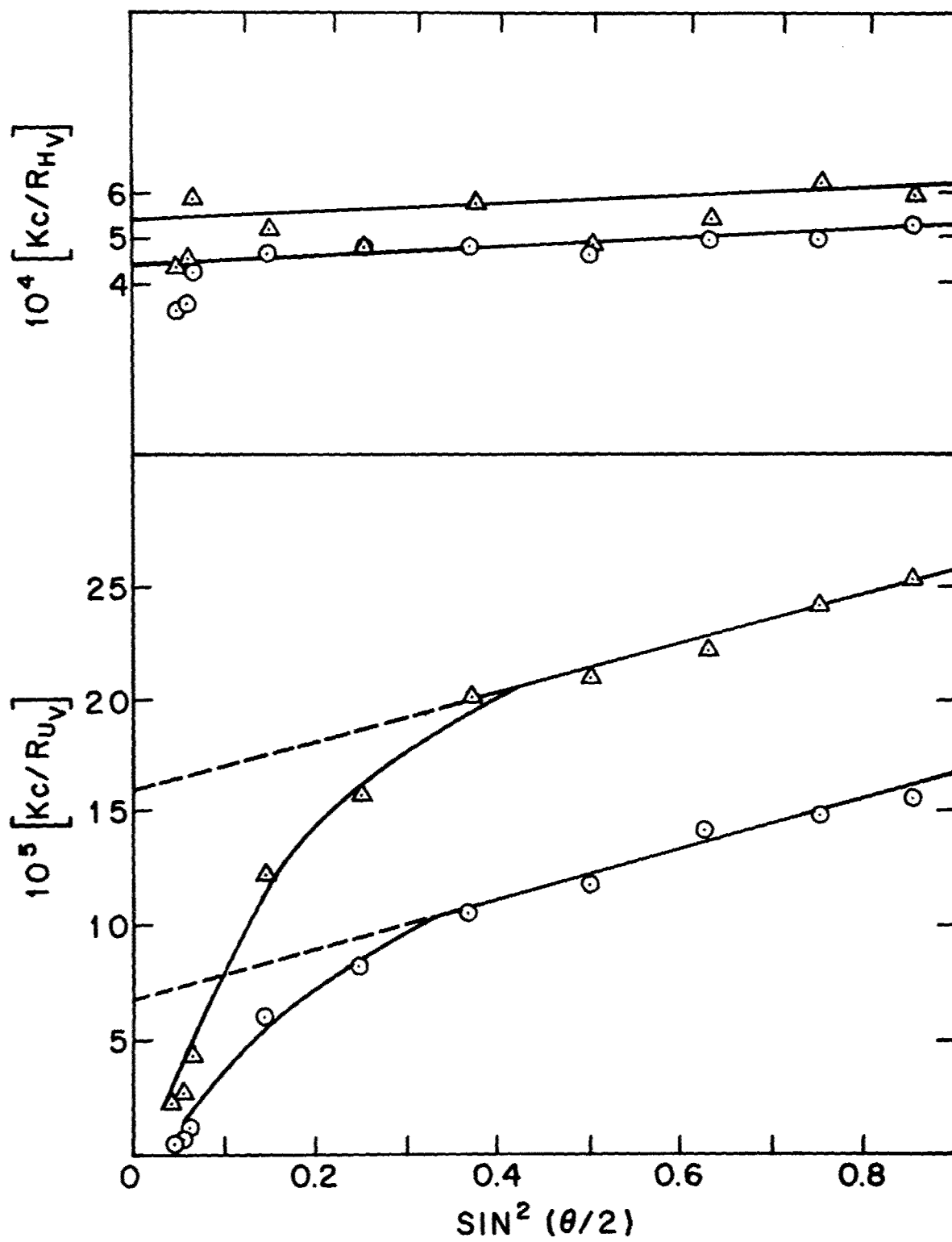


Figure 19 Reciprocal scattering for CMU PBO 160/3 in chlorosulfonic acid. Symbols the same as in Fig. 18.

If carried to equilibrium, the centrifugation would result in a concentration gradient along the length of the cell, with the concentration c_1 and c_2 at the extrema given by (for the idealized case)

$$\ln c_2/c_1 = M_w \frac{\partial \rho}{\partial c} \omega^2 (r_2^2 - r_1^2) / 2RT \quad (70)$$

where r_2 and r_1 are the radii at the extrema, ω is the angular velocity and $\partial \rho / \partial c \simeq 1 - v_p$ is the 'buoyancy factor'. With reasonable values of $\partial \rho / \partial c$ and M_w , use of Eqn. (70) indicates that c_2 and c_1 , should be at most 20 percent apart at equilibrium for the ω used (8,000 rpm). Moreover, it is unlikely that equilibrium was achieved for the centrifugation time used (10-20 h) with the imprecise control of ω and temperature obtaining in the preparative centrifuge used.

Values of D_M were measured for cell positions of 13 and 14 cm ($r_1 \sim 10$ and $r_2 \sim 15$ cm) after 12 hours of centrifugation with the results shown in Fig. 19. It can be seen that Ξ_{LS}^0 differs by a factor of 1.56, with Ξ_{LS}^0 being larger for the lower cell position. For rodlike polymers the sedimentation constant S given by

$$S = \frac{M}{\Xi_{LS}^0} \frac{\partial \rho}{\partial c} \quad (71)$$

depends only weakly on molecular weight. However, S for rodlike chains is nearly proportional to M_L :

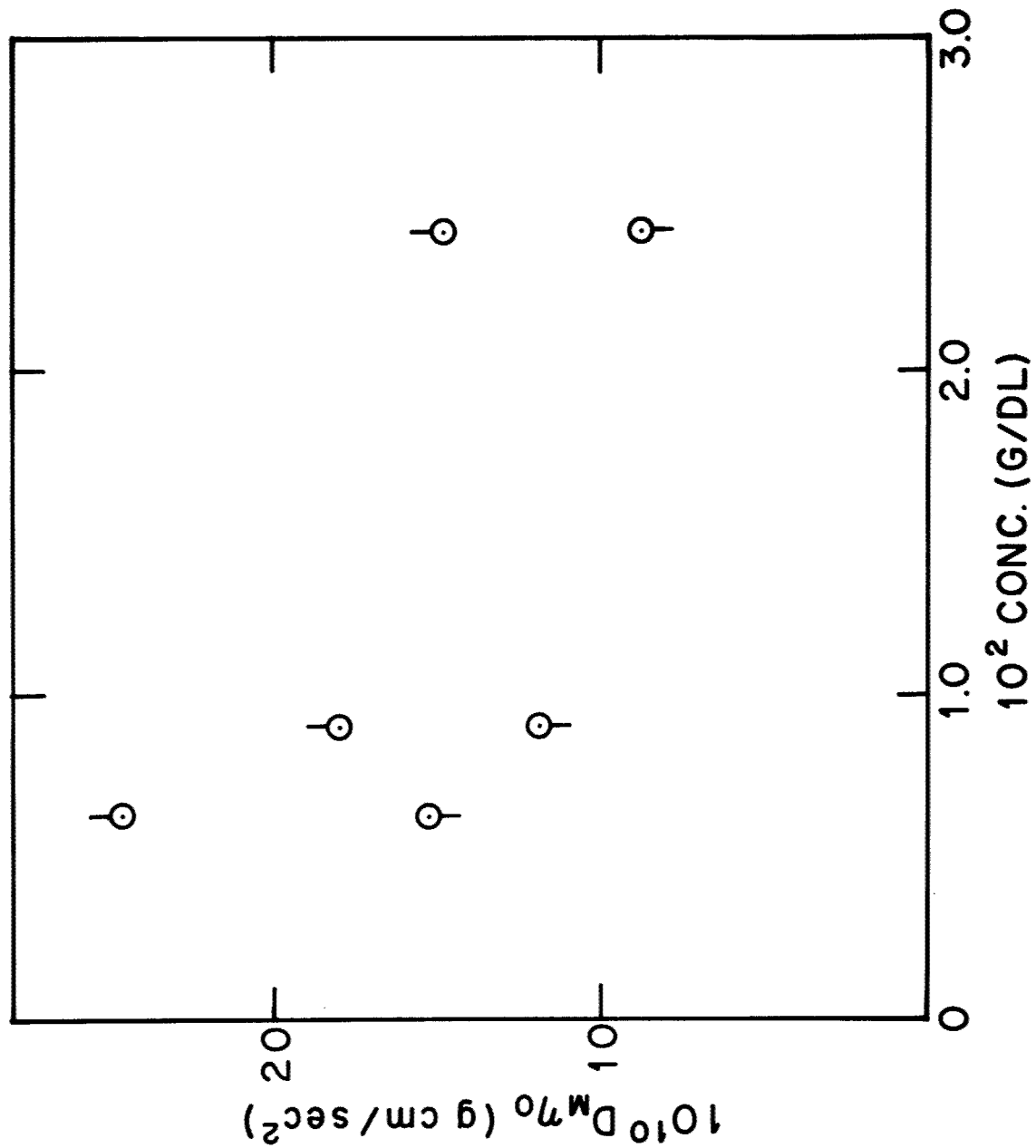


Figure 20 $D_M \eta_0$ for CMU PBO 160/8 in methane sulfonic acid after centrifugation. Pips up: upper portion of cell; pips down: lower portion of cell.

$$S = \frac{M_L}{3\pi\eta_0} H(L/d_H) \approx \frac{M_L}{3\pi\eta_0} \ln L/d_H \quad (72)$$

Consequently, the variation of D_M with cell position after centrifugation may reflect differences in the degree of association of chains associated in parallel array. With this model, the aggregates in the lower part of the cell would have a length about 60 percent longer on the average than the species at the upper part of the cell.

4.5 Estimates of the Rod Length: Values of L_w and $(L_z L_{z+1})^{1/2}$ estimated from various experiments are given in Table 3. The most complete set of data are those for PBO-MIS-160/8, for which it can be seen that the estimates for L_w vary widely as calculated for the relations for rodlike chains. Moreover, a systematic difference obtains between L_w estimated from GPC and $[\eta]$ for almost all of the polymers. (The large value of δ makes it unlikely that the chain conformation deviates much from a rodlike structure, e.g. for $\delta = 0.6$, the minimum value L/ρ would be about unity and if $\delta_0 < 1$, L/ρ would have to be smaller. Interestingly, for MIS-160/8, among the estimates of L_w from GPC, and \bar{M}_{LS}^0 are in best agreement.) The former is obtained with very low polymer concentration, and the latter is nearly independent of M_L . Thus, these estimates would be as nearly free of the effects of association as any of the experimental values. If the chains associate in parallel array, the value of $[\eta]$ would be decreased, by a factor about equal to the degree of association ν reflecting the decrease in the number of species giving

TABLE 3
Summary of Average Length of PBO and PBT Polymers

Polymer	δ	GPC	L_w , Calculated From				$[Kc/R_{VV}(0)]^0$	UV Q	GPC	$(L_{z+1})^{1/2}$	$\langle s^2 \rangle_{HV}$	$\langle s^2 \rangle_{UV}$
			L_η	L_{Ξ}	$L_{\eta\Xi}$	$L_{\eta\Xi}$						
PBO-MIS-160/8	0.6	930	445	745	300	1200	1100	1650	1070	1550		
PBO-AFML-9	0.6	--	440	--	--	--	1000	--	--	1900		
PBO-AFML-2	--	620	370	--	--	--	--	980	--	--		
PBO-AFML-5	0.6	565	330	--	--	--	840	880	--	1600		
PBO-AFML-6	--	330	210	--	--	--	660	570	--	--		
PBO-CEL-9A	--	770	430	--	--	--	--	1300	--	--		
PBO-CEL-3	--	340	370	--	--	--	--	450	--	--		
PBT-SRI-73	--	--	910	300	2370	1200	1040	--	1020	1510		
PBT-SRI-20	--	950	650	--	--	1100	960	1200	870	1440		

rise to the viscous loss. Thus, the value of M_L in Eqns. (21) and (22) should be replaced by νM_L , where M_L is the mass per unit length of the undissociated chain. For MIS-160/8, it appears that with $\nu = 2.8$, values of L_w calculated from L_{η} and $L_{\eta, \Xi}$ are then in reasonable agreement with L_w from the GPC and L_{Ξ} .

Alternatively, one might inquire whether the low value of, for example, $L_{\eta, \Xi}$ could be caused by deviation from rodlike chain conformation. For chains with intermediate L/ρ , the functions $w(L/\rho)$ in Eqn. (1) and $H(L/\rho, L/d_H)$ in Eqn. (5) cannot be replaced by their limiting values for small L/ρ for rodlike chains. For example, expansion of the former for small L/ρ gives

$$R_G^2 = \frac{L^2}{12} \left[1 - \frac{1}{5}(L/\rho) + \frac{1}{30}(L/\rho)^2 - \dots \right] \quad (73)$$

Estimates of R_G from Eqns. (1) and (73) are within 2 percent for L/ρ less than 2. It may be remembered that for PBO, the observed values of δ indicate that L/ρ is no larger than unity, and perhaps much less than unity if δ is less than unity. For $L/\rho < 1$, $H(L/\rho, L/d_H)$ is essentially equal to $H(L/d_H)$. Consequently, the substantial deviation of L_w calculated from $L_{\eta, \Xi}$ from the estimate based on GPC data is too large to be attributed to departure from a strictly rodlike conformation, even if L/ρ has its maximum value of unity for PBO. Indeed, the relative insensitivity of H/F to $L/\rho < 1$ provided part of the motivation for interest in $L_{\eta, \Xi}$, and the need to involve interchain association to explain the results for $L_{\eta, \Xi}$.

The reported values of L_w based on AILS measurements of R_{Vv} or R_{Uv} are biased by neglect of data for scattering angles less than about 50 deg. As discussed in a previous section, use of the low angle data would give a large value for M_w and $\langle s^2 \rangle_{APP,U}$, reflecting the presence of a small amount of some large (aggregated) species. Consequently, comparison of these values of L_w with those based on R_{Hv} , L_η or $L_{\eta,\Xi}$ cannot be unequivocal. For example, the estimate of $L_w = 1200 \text{ \AA}$ based on $[Kc/R_{Uv}(0)]^0$ may reflect some interchain association even though $Kc/R_{Uv}(0)$ was obtained by extrapolations neglecting data for scattering angle less than ca 50 deg.

4.6 Phase Equilibria in Moderately Concentrated Solutions: Both PBO and PBT will form nematic liquid crystalline solutions in $\text{CH}_3\text{SO}_3\text{H}$ or ClSO_3H under appropriate conditions of concentration and temperature. According to Flory and coworkers, (athermal) solutions of rodlike polymers with polymer volume fraction ϕ will be isotropic provided ϕ is less than some critical value ϕ_c (more precisely, ϕ_c is the threshold concentration required for incipient separation of an ordered phase from an isotropic solution). For a rodlike polymer with a most probable distribution of lengths ($L_w/L_n = 2$, etc.), ϕ_c may be expressed in terms of the number average aspect ratio x :¹⁶

$$\phi_c = p^{-1} \ln p^{-1} \quad (74a)$$

$$x_n = (1 - p)^{-1} \quad (74b)$$

or, for large x_n ,

$$\varphi_c \sim \frac{1}{x_n} \quad (74c)$$

In comparison, for a monodispersed rodlike polymer¹⁷

$$\varphi_c = \frac{8}{x} \left(1 - \frac{2}{x}\right) \approx \frac{8}{x} \quad (75)$$

Both Eqns. (74 and 75) apply to athermal solutions, so that, for example, φ_c is expected to be independent of temperature or solvent. The approximately eight-fold decrease in φ_c for a polymer with a most probable distribution as compared with the monodisperse case reflects preferential separation of the longer chains in the distribution with the former. Indeed, Flory and coworkers predict¹⁶ that the chains will be portioned between the two phases according to chain length. The phase equilibria of moderately concentrated solutions of PBO and PBT have been studied using polarized light microscopy. In these experiments, a solution was placed in the cell shown in Fig. 20 by drawing the solution up through a Teflon tube attached to the Luer fitting; the solution was not allowed to enter the tube leading to the vacuum. The latter tube was sealed by fusing the glass, and the Luer fitting was closed using a Teflon stopcork. Solutions so sealed remain free of moisture induced coagulation indefinitely.

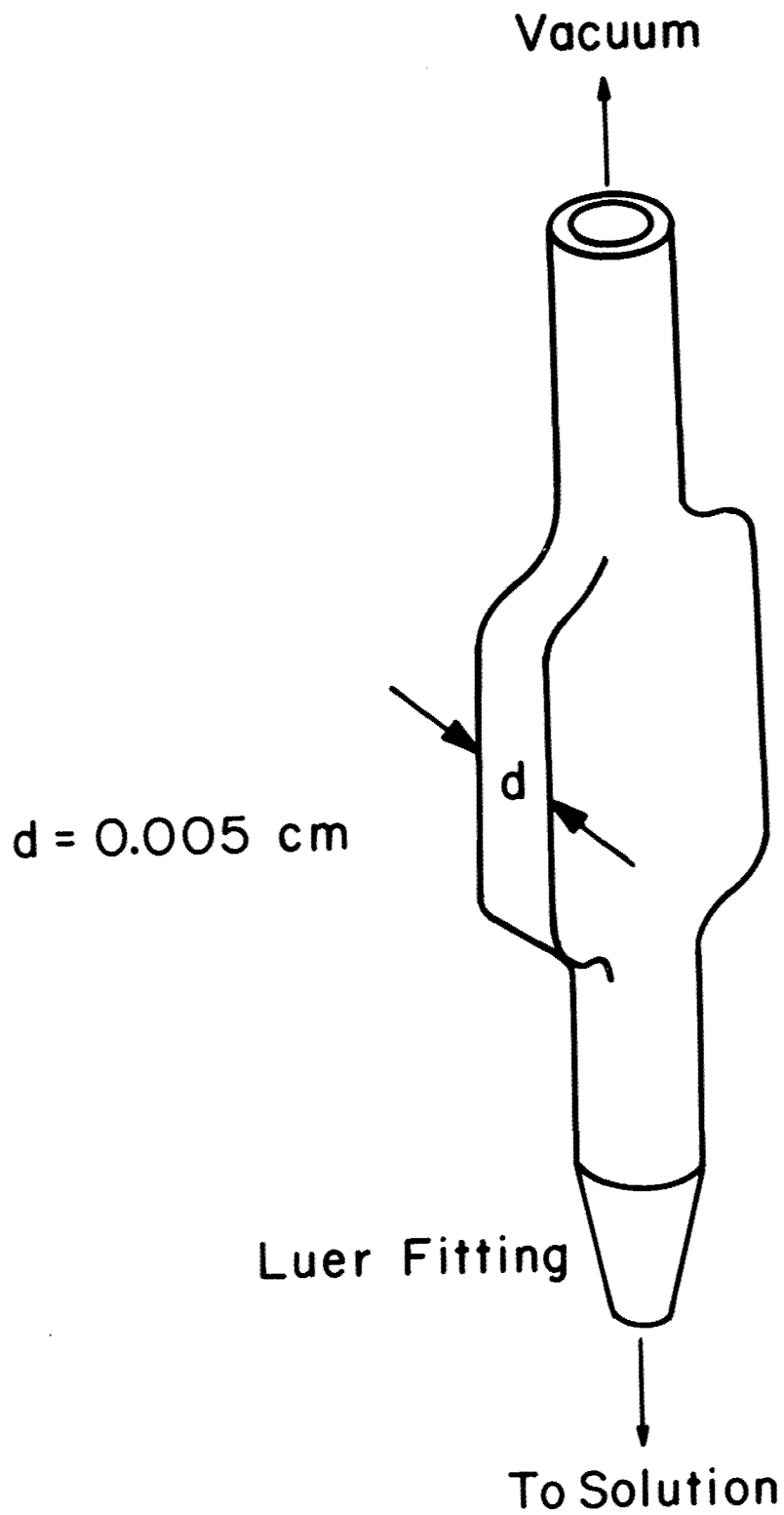


Figure 21 Cell for observation of phase changes.

The sealed cell can be fitted into the thermostatted stage of a polarizing microscope for determination of the phase diagram for the solution over a temperature range of about 0° to 120° C. Results for two PBT polymers are shown in Fig. 21. The phase diagram can be characterized by the temperature interval ΔT_{φ} for biphasic stability for a solution with polymer volume fraction φ , and the concentration interval $\Delta \varphi_T$ for biphasic stability for solutions at temperature T. Presently, the most complete set of data available is for solutions of PBT-SRI-53 in ClSO_3H , ($[\eta] = 14.0$ in $\text{CH}_3\text{SO}_3\text{H}$). As may be seen in Fig. 21, the intervals ΔT_{φ} and $\Delta \varphi_T$ are narrow for this polymer, and the phase diagram exhibits concave curvature over the range of T and φ explored. The latter appears to be typical behavior for solutions of rodlike polymers in protic acid solvents. Less complete data are available for solutions of PBT-SRI-20 in ClSO_3H and $\text{CH}_3\text{SO}_3\text{H}$. ($[\eta] = 6.2$ in $\text{CH}_3\text{SO}_3\text{H}$). As shown in Fig. 21, $\Delta \varphi_T$ tends to be somewhat larger for this lower molecular weight polymer, and surprisingly, the concentration interval for the biphasic solution is different with the two solvents used. Similar, if less complete, behavior is exhibited by PBO solutions as may be seen in Table 4.

An estimate for φ_c for PBT-SRI-20 calculated with Eqn. (74), with $x_n = M_n/M_L = 65$ is shown in the range of the concentration for the onset of anisotropy determined experimentally but since the latter varies with temperature, a meaningful comparison with φ_c calculated with Eqn. (74) is not feasible.

Neither the temperature dependence observed for the phase

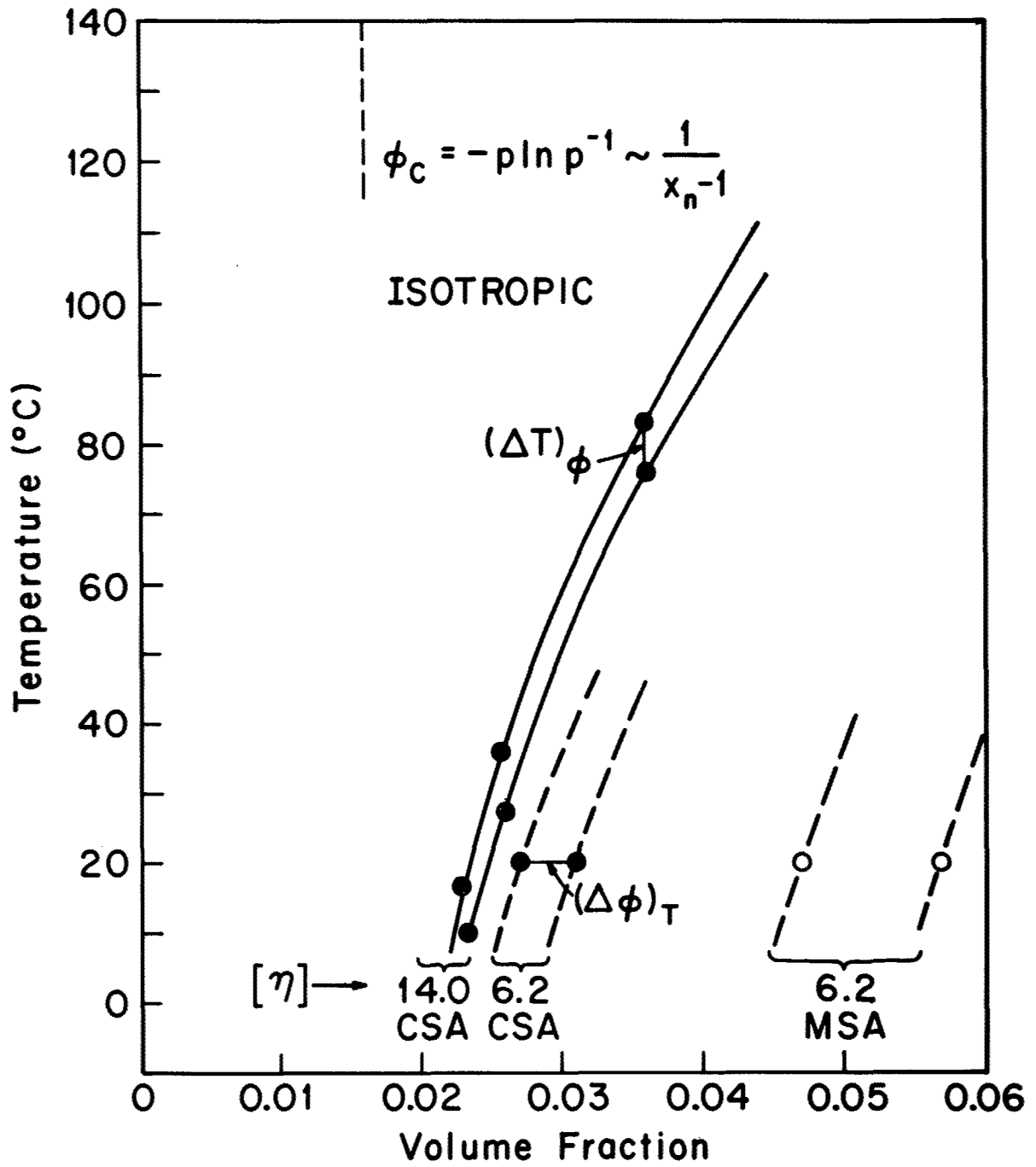


Figure 22 Temperature and concentration limits of the biphasic region for PBT solutions.

TABLE 4

Temperature and Concentration Ranges For
Biphasic Solution in PBO and PBT Polymers

POLYMER	SOLVENT SYSTEM	VOLUME FRACTION	$(\Delta T)_\phi$	TEMPERATURE	$(\Delta \phi)_T$
PBT-53 [η] = 14.0 dl/g	CSA	0.0226	6°C	20°C	0.0015
	CSA	0.026	9°C		
	CSA	0.036	7°C	80°C	0.002
PBO-5 [η] = 2.5 dl/g	MSA	0.075	105°C		
PBO-37 [η] = 2.2 dl/g	CSA	0.070	101°C		
	MSA + 2.5% CSA	0.081	50°C		

diagram or the variation with concentration can be represented by the athermal mixing models used to derive Eqn. (74). Possible explanation for the observed behavior could include (orientational dependent) intermolecular interactions and/or intermolecular association. For example, if the rodlike chains are aggregated in parallel arrays with ν molecules per bundle, then the effective number of species is decreased, with some concomitant decrease in the effective L/d ratio. This effect could account for the observed increase in the concentration range for biphasic stability in $\text{CH}_3\text{SO}_3\text{H}$ solutions as compared with solutions in ClSO_3H . It is expected that this behavior will become better understood as additional data are acquired in future studies.

5. CONCLUSIONS AND SUMMARY

The characterization of PBO and PBT by the physical chemical methods described above shows that both can be regarded as rod-like polymers, but that interpretation of the physical chemical data is complicated by the effects of intermolecular association. The latter leads to aggregated states that are probably not at equilibrium, so that the physical chemical data can be influenced by the association in ways that are both difficult to reproduce and interpret. Consequently, it is generally necessary to use a combination of physical methods to characterize the properties of the rod-like chains. Methods used in this study include absolute intensity and intensity fluctuation light scattering (AALS and IFLS), viscometry and absorption and fluorescence spectroscopy. With the AALS measurements, the analysis of the depolarized scattering components proves to be very useful, providing rather direct evidence of extended chain conformation.

Owing to the tendency for intermolecular association, it is necessary to use strong, protic solvents to dissolve PBO and PBT. These protonate the chain so that the resultant solution properties are sensitive to the ionic strength of the system. It is shown that this has profound effect on the concentration dependence of the solution properties measured by AALS, IFLS and viscometry. When the ionic strength is very low, the electrostatic interactions among the protonated rod-like chains result in strong repulsive interactions. These are so large that reliable extrapolation to infinite dilution may be impossible if the ionic strength is low enough (as with solutions in chlorosulfonic acid, for example). On the other hand, if the ionic strength is too

large, it appears that interchain association is favored. In general, the tendency for association appears to be smaller with PBT than with PBO.

REFERENCES

1. H. Yamakawa, "Modern Theory of Polymer Solutions", Herpe and Row, New York, 1971, p. 56.
2. K. Naqai, Polymer Journal, 3, 67 (1972).
3. H. Yamakawa and W. Stockmayer, J. Chem. Phys., 57, 2843 (1972).
4. B. H. Zimm, J. Chem. Phys., 14, 164 (1946).
5. H. Yamakawa and M. Fujii, Macromolecules, 6, 407 (1973).
6. H. Yamakawa and M. Fujii, Macromolecules, 7, 128 (1974).
7. P. Horn, Ann. Phys., 10, 386 (1955).
8. G. C. Berry, J. Poly. Sci., Pol. Symp. Ed., 65, 143 (1978).
9. B. J. Berne and R. Pecora, "Dynamic Light Scattering", Wiley-Interscience, New York, 1976, Ch. 5.
10. G. D. J. Phillies, G. B. Benedek and N. A. Mazer, J. Chem. Phys., 65 (5), 1883-92 (1976).
11. D. J. R. Laurence, "Physical Methods in Macromolecular Chemistry", B. Carroll, Ed., Dekker, New York, 1969, Ch. 5.
12. H. Yamakawa, "Modern Theory of Polymer Solutions", Harper and Row, New York, 1971, p. 327.
13. J. B. Birks, "Photophysics of Aromatic Molecules", Wiley-Interscience, New York, 1970, p. 441.
14. E. F. Casassa, Macromolecules, 9, 182 (1976).
15. D. B. Cotts, and G. C. Berry, Polymer Preprints, 20(2), p. 570 (1979).
16. P. J. Flory and R. S. Frost, Macromolecules, 11, 1126 (1978).
17. P. J. Flory, Proc. Royal Society, Sec. A, 233, 73, (1956).

APPENDIX

The various averages of the molecular weight M_n , M_w , M_z , etc. can be expressed generally as

$$M_k \equiv \frac{\int_0^\infty M^{k+1} f(M) dM}{\int_0^\infty M^k f(M) dM} \quad (1A)$$

where $f(M)$ is the weight fraction of molecules of molecular weight M and

$$\int_0^\infty f(M) dM = 1 \quad (2A)$$

Thus, $M_n = M_{-1}$, $M_w = M_0$, $M_z = M_1$, etc. Exclusion chromatography (GPC) yields the weight fraction of molecules with a given volume expressed as a product $[\eta]M$. Eqn. 21 relating $[\eta]$ and M for a rod-like chain can be used to obtain M from the product $([\eta]M)$:

$$M = M_L \left(\frac{([\eta]M)}{K d_H^{0.2}} \right)^{1/2.8} \quad (3A)$$

Here K is a constant, d_H is the hydrodynamic diameter and M_L is the mass per unit length. Since M_L , d_H and K are independent of molecular weight, they can be removed from the intergration in Eqn. 1A:

$$M_k = \frac{M_L}{(K d_H^{0.2})^{1/2.8}} \frac{\int_0^\infty ([\eta]M)^{(k+1)/2.8} \frac{f(M) dM}{f(M) dM}}{\int_0^\infty ([\eta]M)^{k/2.8} \frac{f(M) dM}{f(M) dM}} \quad (4A)$$

Ratios of the various averages M_w/M_n , etc. will, therefore, be independent of values used for M_L , d_H and K .